Control-volume representation of molecular dynamics

E. R. Smith, D. M. Heyes, D. Dini, and T. A. Zaki*

Department of Mechanical Engineering, Imperial College London, Exhibition Road, London SW7 2AZ, United Kingdom

(Received 13 October 2011; revised manuscript received 2 March 2012; published 22 May 2012)

A molecular dynamics (MD) parallel to the control volume (CV) formulation of fluid mechanics is developed by integrating the formulas of Irving and Kirkwood [J. Chem. Phys. **18**, 817 (1950)] over a finite cubic volume of molecular dimensions. The Lagrangian molecular system is expressed in terms of an Eulerian CV, which yields an equivalent to Reynolds' transport theorem for the discrete system. This approach casts the dynamics of the molecular system into a form that can be readily compared to the continuum equations. The MD equations of motion are reinterpreted in terms of a Lagrangian-to-control-volume ($\mathcal{LCV}$) conversion function ϑ_i for each molecule i. The $\mathcal{LCV}$ function and its spatial derivatives are used to express fluxes and relevant forces across the control surfaces. The relationship between the local pressures computed using the volume average [Lutsko, J. Appl. Phys. **64**, 1152 (1988)] techniques and the method of planes [Todd *et al*., Phys. Rev. E **52**, 1627 (1995)] emerges naturally from the treatment. Numerical experiments using the MD CV method are reported for equilibrium and nonequilibrium (start-up Couette flow) model liquids, which demonstrate the advantages of the formulation. The CV formulation of the MD is shown to be exactly conservative and is, therefore, ideally suited to obtain macroscopic properties from a discrete system.

DOI: 10.1103/PhysRevE.85.056705 PACS number(s): 05.20.−y, 47.11.Mn, 31.15.xv

I. INTRODUCTION

The macroscopic and microscopic descriptions of mechanics have traditionally been studied independently. The former invokes a continuum assumption and aims to reproduce the large-scale behavior of solids and fluids, without the need to resolve the microscale details. On the other hand, molecular simulation predicts the evolution of individual, but interacting, molecules, which has application in nano- and microscale systems. Bridging these scales requires a mesoscopic description, which represents the evolution of the average of many microscopic trajectories through phase space. It is advantageous to cast the fluid dynamics equations in a consistent form for the molecular, mesoscale, and continuum approaches. The current works seeks to achieve this objective by introducing a control volume (CV) formulation for the molecular system.

The control volume approach is widely adopted in continuum fluid mechanics, where the Reynolds transport theorem [1] relates Newton's laws of motion for macroscopic fluid parcels to fluxes through a CV. In this form, fluid mechanics has had great success in simulating both fundamental [2,3] and practical [4–6] flows. However, when the continuum assumption fails, or when macroscopic constitutive equations are lacking, a molecular-scale description is required. Examples include nanoflows, moving contact lines, solid-liquid boundaries, nonequilibrium fluids, and evaluation of transport properties such as viscosity and heat conductivity [7].

Molecular dynamics (MD) involves solving Newton's equations of motion for an assembly of interacting discrete molecules. Averaging is required in order to compute properties of interest, e.g., temperature, density, pressure, and stress, which can vary on a local scale especially out of equilibrium [7]. A rigorous link between mesoscopic and continuum properties was established in the seminal work of Irving and Kirkwood [8], who related the mesoscopic Liouville equation to the differential form of continuum fluid mechanics. However, the resulting equations at a point were expressed in terms of the Dirac δ function—a form which is difficult to manipulate and cannot be applied directly in a molecular simulation. Furthermore, a Taylor series expansion of the Dirac δ functions was required to express the pressure tensor. The final expression for pressure tensor is neither easy to interpret nor to compute [9]. As a result, there have been numerous attempts to develop an expression for the pressure tensor for use in MD simulation [9–21]. Some of these expressions have been shown to be equivalent in the appropriate limit. For example, Heyes *et al*. [22]) demonstrated equivalence between the method of planes (MOP) (Todd *et al*. [13]) and the volume average (VA) (Lutsko [16]) at a surface.

In order to avoid use of the Dirac δ function, the current work adopts a control volume representation of the MD system, written in terms of fluxes and surface stresses. This approach is in part motivated by the success of the control volume formulation in continuum fluid mechanics. At a molecular scale, control volume analyses of NEMD simulations can facilitate evaluation of local fluid properties. Furthermore, the CV method also lends itself to coupling schemes between the continuum and molecular descriptions [23–34].

The equations of continuum fluid mechanics are presented in Sec. II A, followed by a review of the Irving and Kirkwood [8] procedure for linking continuum and mesoscopic properties in Sec. II B. In Sec. III, a Lagrangian-to-control-volume ($\mathcal{LCV}$) conversion function is used to express the mesoscopic equations for mass and momentum fluxes. Section III C focuses on the stress tensor and relates the current formulation to established definitions within the literature [13,16,17]. In Sec. IV, the CV equations are derived for a single microscopic system and subsequently integrated in time in order to obtain a form which can be applied in MD simulations. The conservation properties of the CV formulation are demonstrated in NEMD simulations of Couette flow in Sec. IV C.

*t.zaki@imperial.ac.uk

II. BACKGROUND

This section summarizes the theoretical background. First, the macroscopic continuum equations are introduced, followed by the mesoscopic equations which describe the evolution of an ensemble average of systems of discrete molecules. The link between the two descriptions is subsequently discussed.

A. Macroscopic continuum equations

The continuum conservation of mass and momentum balance can be derived in a Eulerian frame by considering the fluxes through a CV. The mass continuity equation can be expressed as

$$\frac{\partial}{\partial t}\int_V \rho dV = -\oint_S \rho \boldsymbol{u}\cdot d\mathbf{S}, \tag{1}$$

where ρ is the mass density and $\boldsymbol{u}$ is the fluid velocity. The rate of change of momentum is determined by the balance of forces on the CV,

$$\frac{\partial}{\partial t}\int_V \rho \boldsymbol{u} dV = -\oint_S \rho \boldsymbol{u}\boldsymbol{u}\cdot d\mathbf{S} + \mathbf{F}_{\text{surface}} + \mathbf{F}_{\text{body}}. \tag{2}$$

The forces are split into ones which act on the bounding surfaces, $\mathbf{F}_{\text{surface}}$, and body forces, $\mathbf{F}_{\text{body}}$. Surface forces are expressed in terms the pressure tensor, $\boldsymbol{\Pi}$, on the CV surfaces,

$$\mathbf{F}_{\text{surface}} = -\oint_S \boldsymbol{\Pi}\cdot d\mathbf{S}. \tag{3}$$

The rate of change of energy in a CV is expressed in terms of fluxes, the pressure tensor, and a heat flux vector $\mathbf{q}$,

$$\frac{\partial}{\partial t}\int_V \rho\mathcal{E} dV = -\oint_S [\rho\mathcal{E}\boldsymbol{u} + \boldsymbol{\Pi}\cdot\boldsymbol{u} + \mathbf{q}]\cdot d\mathbf{S}, \tag{4}$$

where the energy change due to body forces is not included. The divergence theorem relates surface fluxes to the divergence within the volume, for a variable A,

$$\oint_S \boldsymbol{A}\cdot d\mathbf{S} = \int_V \boldsymbol{\nabla}\cdot\boldsymbol{A} dV. \tag{5}$$

In addition, the differential form of the flow equations can be recovered in the limit of an infinitesimal control volume [35],

$$\boldsymbol{\nabla}\cdot\boldsymbol{A} = \lim_{V\to 0}\frac{1}{V}\oint_S \boldsymbol{A}\cdot d\mathbf{S}. \tag{6}$$

B. Relationship between the continuum and the mesoscopic descriptions

A mesoscopic description is a temporal and spatial average of the molecular trajectories, expressed in terms of a probability function, f. Irving and Kirkwood [8] established the link between the mesoscopic and continuum descriptions using the Dirac δ function to define the macroscopic density at a point $\mathbf{r}$ in space,

$$\rho(\mathbf{r},t) \equiv \sum_{i=1}^{N}\langle m_i\delta(\mathbf{r}_i-\mathbf{r});f\rangle. \tag{7}$$

The angled brackets $\langle\alpha;f\rangle$ denote the inner product of α with f, which gives the expectation of α for an ensemble of systems. The mass and position of a molecule i are denoted m_i and $\mathbf{r}_i$, respectively, and N is the number of molecules in a single system. The momentum density at a point in space is similarly defined by

$$\rho(\mathbf{r},t)\boldsymbol{u}(\mathbf{r},t) \equiv \sum_{i=1}^{N}\langle \mathbf{p}_i\delta(\mathbf{r}_i-\mathbf{r});f\rangle, \tag{8}$$

where the molecular momentum, $\mathbf{p}_i = m_i\dot{\mathbf{r}}_i$. Note that $\mathbf{p}_i$ is the momentum in the laboratory frame and not the peculiar value $\overline{\mathbf{p}}_i$ which excludes the macroscopic streaming term at the location of molecule i, $\boldsymbol{u}(\mathbf{r}_i)$, Ref. [7],

$$\overline{\mathbf{p}}_i \equiv m_i\left[\frac{\mathbf{p}_i}{m_i} - \boldsymbol{u}(\mathbf{r}_i)\right]. \tag{9}$$

The present treatment uses $\mathbf{p}_i$ in the laboratory frame. A discussion of translating CV and its relationship to the peculiar momentum is given in Appendix A.

Finally, the energy density at a point in space is defined by

$$\rho(\mathbf{r},t)\mathcal{E}(\mathbf{r},t) \equiv \sum_{i=1}^{N}\langle e_i\delta(\mathbf{r}_i-\mathbf{r});f\rangle, \tag{10}$$

where the energy of the ith molecule is defined as the sum of the kinetic energy and the intermolecular interaction potential ϕ_{ij},

$$e_i \equiv \frac{p_i^2}{2m_i} + \frac{1}{2}\sum_{j\neq i}^{N}\phi_{ij}. \tag{11}$$

It is implicit in this definition that the potential energy of an interatomic interaction, ϕ_{ij}, is divided equally between the two interacting molecules, i and j.

As phase space is bounded, the evolution of a property, α, in time is governed by the equation,

$$\frac{\partial}{\partial t}\langle\alpha;f\rangle = \sum_{i=1}^{N}\left\langle \mathbf{F}_i\cdot\frac{\partial\alpha}{\partial\mathbf{p}_i} + \frac{\mathbf{p}_i}{m_i}\cdot\frac{\partial\alpha}{\partial\mathbf{r}_i};f\right\rangle, \tag{12}$$

where $\mathbf{F}_i$ is the force on molecule i, and $\alpha = \alpha(\mathbf{r}_i(t),\mathbf{p}_i(t))$ is an implicit function of time. Using Eq. (12), Irving and Kirkwood [8] derived the time evolution of the mass [from Eq. (7)], momentum density [from Eq. (8)], and energy density [from Eq. (10)] for a mesoscopic system. A comparison of the resulting equations to the continuum counterpart provided a term-by-term equivalence. Both the mesoscopic and continuum equations are valid at a point; the former expressed in terms of Dirac δ and the latter in differential form. In the current work, the mass and momentum densities are recast within the CV framework, which avoids use of the Dirac δ functions directly, and attendant problems with their practical implementation.

III. THE CONTROL VOLUME FORMULATION

In order to cast the governing equations for a discrete system in CV form, a "selection function" ϑ_i is introduced, which isolates those molecules within the region of interest. This function is obtained by integrating the Dirac δ function, $\delta(\mathbf{r}-\mathbf{r}_i)$, over a cuboid in space, centered at $\mathbf{r}$ and of side length $\Delta\mathbf{r}$ as illustrated in Fig. 1(a) [37]. Using $\delta(\mathbf{r}_i-\mathbf{r}) = \delta(x_i-x)$

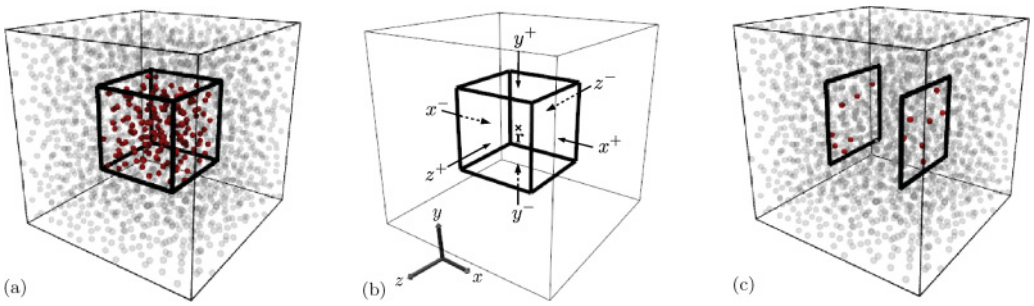

FIG. 1. (Color online) The CV function and its derivative applied to a system of molecules. The figures were generated using the VMD visualization package [36]. From left to right, (a) schematic of ϑ_i which selects only the molecules within a cube; (b) location of cube center $\mathbf{r}$ and labels for cube surfaces; (c) schematic of $\partial\vartheta_i/\partial x$ which selects only molecules crossing the x^+ and x^- surface planes.

$\delta(y_i - y)\delta(z_i - z)$, the resulting triple integral is

$$\begin{aligned}\vartheta_i &\equiv \int_{x^-}^{x^+}\int_{y^-}^{y^+}\int_{z^-}^{z^+}\delta(x_i - x)\delta(y_i - y)\delta(z_i - z)dxdydz \\ &= [[[H(x_i - x)H(y_i - y)H(z_i - z)]_{x^-}^{x^+}]_{y^-}^{y^+}]_{z^-}^{z^+} \\ &= [H(x^+ - x_i) - H(x^- - x_i)] \\ &\times [H(y^+ - y_i) - H(y^- - y_i)] \\ &\times [H(z^+ - z_i) - H(z^- - z_i)], \end{aligned} \tag{13}$$

where H is the Heaviside function, and the limits of integration are defined as $\mathbf{r}^- \equiv \mathbf{r} - \frac{\Delta\mathbf{r}}{2}$ and $\mathbf{r}^+ \equiv \mathbf{r} + \frac{\Delta\mathbf{r}}{2}$ for each direction [see Fig. 1(b)]. Note that ϑ_i can be interpreted as a Lagrangian-to-control-volume conversion function ($\mathcal{LCV}$) for molecule i. It is unity when molecule i is inside the cuboid and equal to zero otherwise, as illustrated in Fig. 1(a). Using L'Hôpital's rule and defining, $\Delta V \equiv \Delta x\Delta y\Delta z$, the $\mathcal{LCV}$ function for molecule i reduces to the Dirac δ function in the limit of zero volume,

$$\delta(\mathbf{r} - \mathbf{r}_i) = \lim_{\Delta V\to 0}\frac{\vartheta_i}{\Delta V}.$$

The spatial derivative in the x direction of the $\mathcal{LCV}$ function for molecule i is

$$\frac{\partial\vartheta_i}{\partial x} = -\frac{\partial\vartheta_i}{\partial x_i} = [\delta(x^+ - x_i) - \delta(x^- - x_i)]S_{xi}, \tag{14}$$

where S_{xi} is

$$\begin{aligned}S_{xi} \equiv\ &[H(y^+ - y_i) - H(y^- - y_i)] \\ &\times [H(z^+ - z_i) - H(z^- - z_i)].\end{aligned} \tag{15}$$

Equation (14) isolates molecules on a 2D rectangular patch in the yz plane. The derivative $\partial\vartheta_i/\partial x$ is only nonzero when molecule i is crossing the surfaces marked in Fig. 1(c), normal to the x direction. The contribution of the ith molecule to the net rate of mass flux through the control surface is expressed in the form, $\mathbf{p}_i \cdot d\mathbf{S}_i$. Defining for the right x surface,

$$dS_{xi}^+ \equiv \delta(x^+ - x_i)S_{xi}, \tag{16}$$

and similarly for the left surface, dS_{xi}^-, the total flux Eq. (14) in any direction $\mathbf{r}$ is, then,

$$\frac{\partial\vartheta_i}{\partial\mathbf{r}} = d\mathbf{S}_i^+ - d\mathbf{S}_i^- \equiv d\mathbf{S}_i. \tag{17}$$

The $\mathcal{LCV}$ function is key to the derivation of a molecular-level equivalent of the continuum CV equations, and it will be used extensively in the following sections. The approach in Secs. III A, III B, and III D shares some similarities with the work of Serrano and Español [38] which considers the time evolution of Voronoi characteristic functions. However, the $\mathcal{LCV}$ function has precisely defined extents which allows the development of conservation equations for a microscopic system. In the following treatment, the CV is fixed in space (i.e., $\mathbf{r}$ is not a function of time). The extension of this treatment to an advecting CV is made in Appendix A.

A. Mass conservation for a molecular CV

In this section, a mesoscopic expression for the mass in a cuboidal CV is derived. The time evolution of mass within a CV is shown to be equal to the net mass flux of molecules across its surfaces.

The mass inside an arbitrary CV at the molecular scale can be expressed in terms of the $\mathcal{LCV}$ as follows:

$$\begin{aligned}\int_V \rho(\mathbf{r},t)dV &= \int_V \sum_{i=1}^{N}\langle m_i\delta(\mathbf{r}_i - \mathbf{r});f\rangle dV \\ &= \sum_{i=1}^{N}\int_{x^-}^{x^+}\int_{y^-}^{y^+}\int_{z^-}^{z^+}\langle m_i\delta(\mathbf{r}_i - \mathbf{r});f\rangle dxdydz \\ &= \sum_{i=1}^{N}\langle m_i\vartheta_i;f\rangle. \end{aligned} \tag{18}$$

Taking the time derivative of Eq. (18) and using Eq. (12),

$$\begin{aligned}\frac{\partial}{\partial t}\int_V \rho(\mathbf{r},t)dV &= \frac{\partial}{\partial t}\sum_{i=1}^{N}\langle m_i\vartheta_i;f\rangle \\ &= \sum_{i=1}^{N}\left\langle\frac{\mathbf{p}_i}{m_i}\cdot\frac{\partial}{\partial\mathbf{r}_i}m_i\vartheta_i + \mathbf{F}_i\cdot\frac{\partial}{\partial\mathbf{p}_i}m_i\vartheta_i;f\right\rangle. \end{aligned} \tag{19}$$

The term $\partial m_i\vartheta_i/\partial\mathbf{p}_i = 0$, as ϑ_i is not a function of $\mathbf{p}_i$. Therefore,

$$\frac{\partial}{\partial t}\int_V \rho dV = -\sum_{i=1}^{N}\left\langle\mathbf{p}_i\cdot\frac{\partial\vartheta_i}{\partial\mathbf{r}};f\right\rangle, \tag{20}$$

where the equality $\partial\vartheta_i/\partial\mathbf{r}_i = -\partial\vartheta_i/\partial\mathbf{r}$ has been used. From the continuum mass conservation given in Eq. (1), the macroscopic and mesoscopic fluxes over the surfaces can be equated,

$$\sum_{\text{faces}}^{6}\int_{S_f}\rho\boldsymbol{u}\cdot d\mathbf{S}_f = \sum_{i=1}^{N}\langle\mathbf{p}_i\cdot d\mathbf{S}_i;f\rangle. \tag{21}$$

The mesoscopic equation for evolution of mass in a control volume is given by

$$\frac{\partial}{\partial t}\sum_{i=1}^{N}\langle m_i\vartheta_i;f\rangle = -\sum_{i=1}^{N}\langle\mathbf{p}_i\cdot d\mathbf{S}_i;f\rangle. \tag{22}$$

Appendix A shows that the surface mass flux yields the Irving and Kirkwood [8] expression for divergence as the CV tends to a point (i.e., $V\to 0$), in analogy to Eq. (6).

B. Momentum balance for a molecular CV

In this section, a mesoscopic expression for time evolution of momentum within a CV is derived. The starting point is to integrate the momentum at a point, given in Eq. (8), over the CV,

$$\int_V\rho(\mathbf{r},t)\boldsymbol{u}(\mathbf{r},t)dV = \sum_{i=1}^{N}\langle\mathbf{p}_i\vartheta_i;f\rangle. \tag{23}$$

Following a similar procedure to that in Sec. III A, the formula (12) is used to obtain the time evolution of the momentum within the CV,

$$\begin{aligned}\frac{\partial}{\partial t}\int_V\rho(\mathbf{r},t)\boldsymbol{u}(\mathbf{r},t)dV &= \frac{\partial}{\partial t}\sum_{i=1}^{N}\langle\mathbf{p}_i\vartheta_i;f\rangle\\ &= \sum_{i=1}^{N}\Bigg\langle\underbrace{\frac{\mathbf{p}_i}{m_i}\cdot\frac{\partial}{\partial\mathbf{r}_i}\mathbf{p}_i\vartheta_i}_{\mathcal{K}_\mathcal{T}} + \underbrace{\mathbf{F}_i\cdot\frac{\partial}{\partial\mathbf{p}_i}\mathbf{p}_i\vartheta_i}_{\mathcal{C}_\mathcal{T}};f\Bigg\rangle,\end{aligned} \tag{24}$$

where the terms $\mathcal{K}_\mathcal{T}$ and $\mathcal{C}_\mathcal{T}$ are the kinetic and configurational components, respectively. The kinetic part is

$$\mathcal{K}_\mathcal{T} = \sum_{i=1}^{N}\left\langle\frac{\mathbf{p}_i}{m_i}\cdot\frac{\partial}{\partial\mathbf{r}_i}\mathbf{p}_i\vartheta_i;f\right\rangle = \sum_{i=1}^{N}\left\langle\frac{\mathbf{p}_i\mathbf{p}_i}{m_i}\cdot\frac{\partial\vartheta_i}{\partial\mathbf{r}_i};f\right\rangle, \tag{25}$$

where $\mathbf{p}_i\mathbf{p}_i$ is the dyadic product. For any surface of the CV, here x^+, the molecular flux can be equated to the continuum convection and pressure on that surface,

$$\begin{aligned}&\int_{S_x^+}\rho(x^+,y,z,t)\boldsymbol{u}(x^+,y,z,t)u_x(x^+,y,z,t)dydz\\ &+\int_{S_x^+}\mathbf{K}_x^+dydz = \sum_{i=1}^{N}\left\langle\frac{\mathbf{p}_i p_{ix}}{m_i}dS_{xi}^+;f\right\rangle,\end{aligned}$$

where $\mathbf{K}_x^+$ is the kinetic part of the pressure tensor due to molecular transgressions across the x^+ CV surface. The average molecular flux across the surface is, then,

$$\{\rho\boldsymbol{u}u_x\}^+ + \mathbf{K}_x^+ = \frac{1}{\Delta A_x^+}\sum_{i=1}^{N}\left\langle\frac{\mathbf{p}_i p_{ix}}{m_i}dS_{xi}^+;f\right\rangle, \tag{26}$$

where the continuum expression $\{\rho\boldsymbol{u}u_x\}^+$ is the average flux through a flat region in space with area $\Delta A_x^+ = \Delta y\Delta z$. This kinetic component of the pressure tensor is discussed further in Sec. III C.

The configurational term of Eq. (24) is

$$\mathcal{C}_\mathcal{T} = \sum_{i=1}^{N}\left\langle\mathbf{F}_i\cdot\frac{\partial}{\partial\mathbf{p}_i}\mathbf{p}_i\vartheta_i;f\right\rangle = \sum_{i=1}^{N}\langle\mathbf{F}_i\vartheta_i;f\rangle, \tag{27}$$

where the total force $\mathbf{F}_i$ on particle i is the sum of pairwise-additive interactions with potential ϕ_{ij}, and from an external potential ψ_i,

$$\vartheta_i\mathbf{F}_i = -\vartheta_i\frac{\partial}{\partial\mathbf{r}_i}\left(\sum_{j\neq i}^{N}\phi_{ij}+\psi_i\right).$$

It is commonly assumed that the potential energy of an interatomic interaction, ϕ_{ij}, can be divided equally between the two interacting molecules, i and j, such that

$$\sum_{i,j}^{N}\vartheta_i\frac{\partial\phi_{ij}}{\partial\mathbf{r}_i} = \frac{1}{2}\sum_{i,j}^{N}\left[\vartheta_i\frac{\partial\phi_{ij}}{\partial\mathbf{r}_i}+\vartheta_j\frac{\partial\phi_{ji}}{\partial\mathbf{r}_j}\right], \tag{28}$$

where the notation $\sum_{i,j}^{N} = \sum_{i=1}^{N}\sum_{j\neq i}^{N}$ has been introduced for conciseness. Therefore, the configurational term can be expressed as

$$\mathcal{C}_\mathcal{T} = \frac{1}{2}\sum_{i,j}^{N}\langle\mathbf{f}_{ij}\vartheta_{ij};f\rangle + \sum_{i=1}^{N}\langle\mathbf{f}_{i_{\text{ext}}}\vartheta_i;f\rangle, \tag{29}$$

where $f_{ij} = -\partial\phi_{ij}/\partial\mathbf{r}_i = \partial\phi_{ji}/\partial\mathbf{r}_j$ and $\mathbf{f}_{i_{\text{ext}}} = -\partial\psi_i/\partial\mathbf{r}_i$. The notation, $\vartheta_{ij}\equiv\vartheta_i-\vartheta_j$, is introduced, which is nonzero only when the force acts over the surface of the CV, as illustrated in Fig. 2.

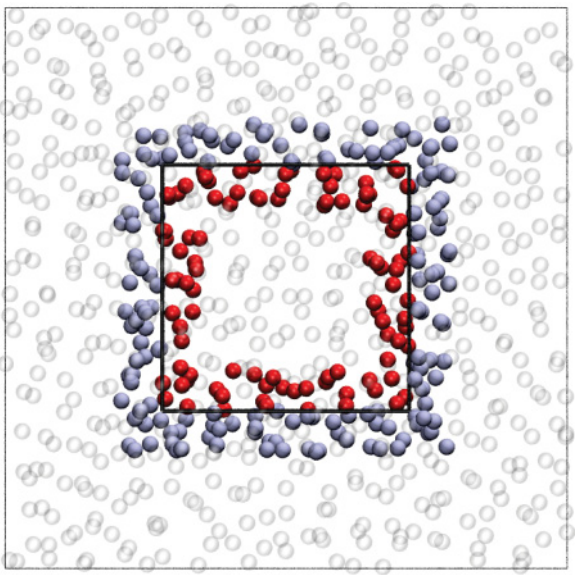

FIG. 2. (Color online) A section through the CV to illustrate the role of ϑ_{ij} in selecting only the i and j interactions that cross the bounding surface of the control volume. Due to the limited range of interactions, only the forces between the internal (red) molecules i and external (blue) molecules j near the surfaces are included.

Substituting the kinetic ($\mathcal{K}_\mathcal{T}$) and configurational ($\mathcal{C}_\mathcal{T}$) terms, from Eqs. (25) and (29) into Eq. (24), the time evolution of momentum within the CV at the mesoscopic scale is

$$\frac{\partial}{\partial t}\sum_{i=1}^{N}\langle \mathbf{p}_i\vartheta_i;f\rangle = -\sum_{i=1}^{N}\left\langle \frac{\mathbf{p}_i\mathbf{p}_i}{m_i}\cdot d\mathbf{S}_i;f\right\rangle + \frac{1}{2}\sum_{i,j}^{N}\langle \mathbf{f}_{ij}\vartheta_{ij};f\rangle + \sum_{i=1}^{N}\left\langle \mathbf{f}_{i_{\text{ext}}}\vartheta_i;f\right\rangle. \quad (30)$$

Equations (22) and (30) describe the evolution of mass and momentum, respectively, within a CV averaged over an ensemble of representative molecular systems. As proposed by Evans and Morriss [7], it is possible to develop microscopic evolution equations that do not require ensemble averaging. Hence, the equivalents of Eqs. (22) and (30) are derived for a single trajectory through phase space in Sec. IV A, integrated in time in Sec. IV B and tested numerically using molecular dynamics simulation in Sec. IV C.

The link between the macroscopic and mesoscopic treatments is given by equating their respective momentum Eqs. (2) and (30),

$$-\oint_S \rho\boldsymbol{uu}\cdot d\mathbf{S} + \mathbf{F}_{\text{surface}} + \mathbf{F}_{\text{body}} = -\sum_{i=1}^{N}\left\langle \frac{\mathbf{p}_i\mathbf{p}_i}{m_i}\cdot d\mathbf{S}_i;f\right\rangle + \frac{1}{2}\sum_{i,j}^{N}\langle \mathbf{f}_{ij}\vartheta_{ij};f\rangle + \sum_{i=1}^{N}\left\langle \mathbf{f}_{i_{\text{ext}}}\vartheta_i;f\right\rangle. \quad (31)$$

As can be seen, each term in the continuum evolution of momentum has an equivalent term in the mesoscopic formulation.

The continuum momentum Eq. (2) can be expressed in terms of the divergence of the pressure tensor, $\boldsymbol{\Pi}$, in the control volume form,

$$\frac{\partial}{\partial t}\int_V \rho\boldsymbol{u}dV = -\oint_S [\rho\boldsymbol{uu}+\boldsymbol{\Pi}]\cdot d\mathbf{S} + \mathbf{F}_{\text{body}} \quad (32a)$$

$$= -\int_V \frac{\partial}{\partial\mathbf{r}}\cdot[\rho\boldsymbol{uu}+\boldsymbol{\Pi}]dV + \mathbf{F}_{\text{body}}. \quad (32b)$$

In the following subsection, the right-hand side of Eq. (31) is recast, first, in divergence form, as in Eq. (32b), and then in terms of surface pressures, as in Eq. (32a).

C. The pressure tensor

The average molecular pressure tensor ascribed to a control volume is conveniently expressed in terms of the $\mathcal{LCV}$ function. This is shown *inter alia* to lead to a number of literature definitions of the local stress tensor. In the first part of this section, the techniques of Irving and Kirkwood [8] are used to express the divergence of the stress [as with the right-hand side of Eq. (32b)] in terms of the intermolecular force. Second, the CV pressure tensor is related to the VA formula [16,17] and, by consideration of the interactions across the surfaces, to the MOP [13,14]. Finally, the molecular CV Eq. (30) is written in analogous form to the macroscopic Eq. (32a).

The pressure tensor, $\boldsymbol{\Pi}$, can be decomposed into a kinetic $\boldsymbol{\kappa}$ term and a configurational stress $\boldsymbol{\sigma}$. In keeping with the engineering literature, the stress and pressure tensors have opposite signs,

$$\boldsymbol{\Pi} = \boldsymbol{\kappa} - \boldsymbol{\sigma}. \quad (33)$$

The separation into kinetic and configurational parts is made to accommodate the debate concerning the inclusion of kinetic terms in the molecular stress [9,39,40].

In order to avoid confusion, the stress, $\boldsymbol{\sigma}$, is herein defined to be due to the forces only (surface tractions). This, combined with the kinetic pressure term $\boldsymbol{\kappa}$, yields the total pressure tensor $\boldsymbol{\Pi}$ first introduced in Eq. (3).

1. Irving-Kirkwood pressure tensor

The virial expression for the stress cannot be applied locally as it is valid only for a homogeneous system [12]. The Irving and Kirkwood [8] technique for evaluating the nonequilibrium, locally defined stress resolves this issue and is herein extended to a CV. To obtain the stress, σ, the intermolecular force term of Eq. (31) is defined to be equal to the divergence of stress,

$$\int_V \frac{\partial}{\partial\mathbf{r}}\cdot\boldsymbol{\sigma}dV \equiv \frac{1}{2}\sum_{i,j}^{N}\langle \mathbf{f}_{ij}\vartheta_{ij};f\rangle = \frac{1}{2}\sum_{i,j}^{N}\int_V \langle \mathbf{f}_{ij}[\delta(\mathbf{r}_i-\mathbf{r})-\delta(\mathbf{r}_j-\mathbf{r})];f\rangle dV. \quad (34)$$

Irving and Kirkwood [8] used a Taylor expansion of the Dirac δ functions to express the pair force contribution in the form of a divergence,

$$\mathbf{f}_{ij}[\delta(\mathbf{r}_i-\mathbf{r})-\delta(\mathbf{r}_j-\mathbf{r})] = -\frac{\partial}{\partial\mathbf{r}}\cdot\mathbf{f}_{ij}\mathbf{r}_{ij}O_{ij}\delta(\mathbf{r}_i-\mathbf{r}),$$

where $\mathbf{r}_{ij}=\mathbf{r}_i-\mathbf{r}_j$, and O_{ij} is an operator which acts on the Dirac δ function,

$$O_{ij} \equiv \left[1-\frac{1}{2}\mathbf{r}_{ij}\frac{\partial}{\partial\mathbf{r}_i}+\cdots-\frac{1}{n!}\left(\mathbf{r}_{ij}\frac{\partial}{\partial\mathbf{r}_i}\right)^{n-1}+\cdots\right]. \quad (35)$$

Equation (34) therefore can be rewritten,

$$\int_V \frac{\partial}{\partial\mathbf{r}}\cdot\boldsymbol{\sigma}dV = -\frac{1}{2}\sum_{i,j}^{N}\int_V\left\langle \frac{\partial}{\partial\mathbf{r}}\cdot\mathbf{f}_{ij}\mathbf{r}_{ij}\,O_{ij}\delta(\mathbf{r}_i-\mathbf{r});f\right\rangle dV. \quad (36)$$

The Taylor expansion in Dirac δ functions is not straightforward to evaluate. This operation can be bypassed by integrating the position of the molecule i over phase space [11] or by replacing the Dirac δ with a similar but finite-valued function of compact support [15,18,19,21]. In the current treatment, the $\mathcal{LCV}$ function, ϑ, is used, which is advantageous because it explicitly defines both the extent of the CV and its surface fluxes. The pressure tensor can be written in terms of the $\mathcal{LCV}$ function by exploiting the following identities (see Appendix of Ref. [8]),

$$O_{ij}\delta(\mathbf{r}_i-\mathbf{r}) = \int_0^1 \delta(\mathbf{r}-\mathbf{r}_i+s\mathbf{r}_{ij})ds. \quad (37)$$

Equation (36) therefore can be written as

$$\int_V \frac{\partial}{\partial \mathbf{r}} \cdot \boldsymbol{\sigma} dV = -\int_V \frac{1}{2} \sum_{i,j}^{N} \left\langle \frac{\partial}{\partial \mathbf{r}} \cdot \mathbf{f}_{ij}\mathbf{r}_{ij} \int_0^1 \delta(\mathbf{r} - \mathbf{r}_i + s\mathbf{r}_{ij}) ds; f \right\rangle dV. \tag{38}$$

Equation Eq. (38) leads to the VA and MOP definitions of the pressure tensor.

2. VA pressure tensor

The VA definition of the stress tensor of Lutsko [16] and Cormier *et al.* [17] can be obtained by rewriting Eq. (38) as

$$\frac{\partial}{\partial \mathbf{r}} \cdot \int_V \boldsymbol{\sigma} dV = -\frac{\partial}{\partial \mathbf{r}} \cdot \int_V \frac{1}{2} \sum_{i,j}^{N} \left\langle \mathbf{f}_{ij}\mathbf{r}_{ij} \int_0^1 \delta(\mathbf{r} - \mathbf{r}_i + s\mathbf{r}_{ij}) ds; f \right\rangle dV. \tag{39}$$

Equating the expressions inside the divergence on both sides of Eq. (39) [41], and assuming the stress is constant within an arbitrary local volume, ΔV, gives an expression for the VA stress,

$$\overset{\text{VA}}{\boldsymbol{\sigma}} = -\frac{1}{2\Delta V} \int_V \sum_{i,j}^{N} \left\langle \mathbf{f}_{ij}\mathbf{r}_{ij} \int_0^1 \delta(\mathbf{r} - \mathbf{r}_i + s\mathbf{r}_{ij}) ds; f \right\rangle dV. \tag{40}$$

Swapping the order of integration and evaluating the integral of the Dirac δ function over ΔV gives a different form of the $\mathcal{LCV}$ function, ϑ_s,

$$\begin{aligned} \vartheta_s &\equiv \int_V \delta(\mathbf{r} - \mathbf{r}_i + s\mathbf{r}_{ij}) dV \\ &= [H(x^+ - x_i + sx_{ij}) - H(x^- - x_i + sx_{ij})] \\ &\quad \times [H(y^+ - y_i + sy_{ij}) - H(y^- - y_i + sy_{ij})] \\ &\quad \times [H(z^+ - z_i + sz_{ij}) - H(z^- - z_i + sz_{ij})], \end{aligned} \tag{41}$$

which is nonzero if a point on the line between the two molecules, $\mathbf{r}_i - s\mathbf{r}_{ij}$, is inside the cubic region (cf. $\mathbf{r}_i$ with ϑ_i). Substituting the definition, ϑ_s [Eq. (41)], into Eq. (40) gives

$$\overset{\text{VA}}{\boldsymbol{\sigma}} = -\frac{1}{2\Delta V} \sum_{i,j}^{N} \langle \mathbf{f}_{ij}\mathbf{r}_{ij} l_{ij}; f \rangle, \tag{42}$$

where l_{ij} is the integral from r_i ($s = 0$) to r_j ($s = 1$) of the ϑ_s function,

$$l_{ij} \equiv \int_0^1 \vartheta_s ds.$$

Therefore, l_{ij} is the fraction of the interaction length between i and j which lies within the CV, as illustrated in Fig. 3. The definition of the configurational stress in Eq. (42) is the same as in the work of Lutsko [16] and Cormier *et al.* [17]. The microscopic divergence theorem given in Appendix A can

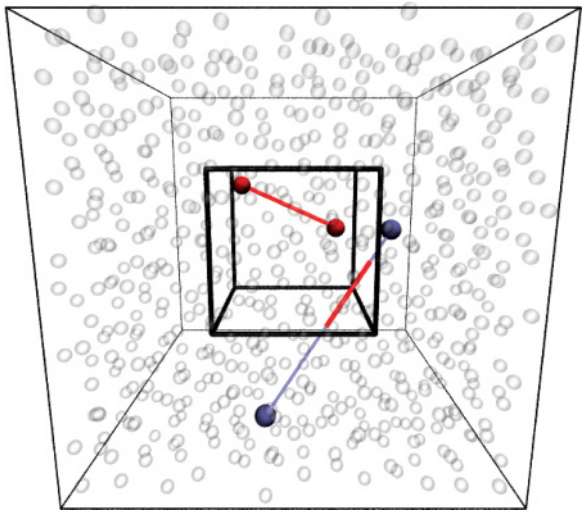

FIG. 3. (Color online) A plot of the interaction length given by the integral of the selecting function ϑ_s defined in Eq. (41) along the line between r_i and r_j. The cases shown are for two molecules which are (a) both inside the volume ($l_{ij} = 1$) and (b) both outside the volume with an interaction crossing the volume, where l_{ij} is the fraction of the total length between i and j inside the volume. The line is thin (blue) outside and thicker (red) inside the volume.

be applied to obtain the volume averaged kinetic component of the pressure tensor, $\mathcal{K}_\mathcal{T}$, in Eq. (25),

$$\sum_{i=1}^{N} \left\langle \frac{\mathbf{p}_i\mathbf{p}_i}{m_i} \cdot d\mathbf{S}_i; f \right\rangle = \frac{\partial}{\partial \mathbf{r}} \cdot \sum_{i=1}^{N} \overbrace{\left\langle \frac{\mathbf{p}_i\mathbf{p}_i}{m_i} \vartheta_i; f \right\rangle}^{\overset{VA}{\{\boldsymbol{\rho uu}\}} + \overset{VA}{\boldsymbol{\kappa}}}.$$

Note that the expression inside the divergence includes both the advection, $\overset{VA}{\{\boldsymbol{\rho uu}\}}$, and kinetic components of the pressure tensor. The VA form [17] is obtained by combining the above expression with the configurational stress $\overset{\text{VA}}{\boldsymbol{\sigma}}$,

$$\begin{aligned} \overset{VA}{\{\boldsymbol{\rho uu}\}} + \overset{VA}{\boldsymbol{\kappa}} - \overset{\text{VA}}{\boldsymbol{\sigma}} &= \overset{VA}{\{\boldsymbol{\rho uu}\}} + \overset{VA}{\boldsymbol{\Pi}} \\ &= \frac{1}{\Delta V} \sum_{i=1}^{N} \left\langle \frac{\mathbf{p}_i\mathbf{p}_i}{m_i} \vartheta_i + \frac{1}{2} \sum_{i,j}^{N} \mathbf{f}_{ij}\mathbf{r}_{ij} l_{ij}; f \right\rangle. \end{aligned} \tag{43}$$

In contrast to the work of Cormier *et al.* [17], the advection term in the above expression is explicitly identified in order to be compatible with the right-hand side of Eq. (32b) and the definition of the pressure tensor, $\boldsymbol{\Pi}$.

3. MOP pressure tensor

The stress in the CV can also be related to the tractions over each surface. In analogy to differentiation of the molecular $\mathcal{LCV}$ function, ϑ_i, to evaluate the flux, the stress $\mathcal{LCV}$ function, ϑ_s, can be differentiated to give the tractions over each surface. These surface tractions are the ones used in the formal definition of the continuum Cauchy stress tensor. The surface traction (i.e., force per unit area) and the kinetic pressure on a surface combined give the MOP expression for the pressure tensor [13].

In the context of the CV, the forces and fluxes on the six bounding surfaces are required to obtain the pressure inside the CV. It is herein shown that each face takes the form of the Han and Lee [14] localization of the MOP pressure components. The divergence theorem is used to express the left-hand side of Eq. (38) in terms of stress across the six faces of the cube. The mesoscopic right-hand side of Eq. (38) can also be expressed as surface stresses by starting with the $\mathcal{LCV}$ function ϑ_s,

$$\sum_{\text{faces}}^{6}\int_{S_f}\boldsymbol{\sigma}\cdot d\mathbf{S}_f=-\frac{1}{2}\sum_{i,j}^{N}\left\langle \mathbf{f}_{ij}\mathbf{r}_{ij}\cdot\int_0^1\frac{\partial\vartheta_s}{\partial\mathbf{r}}ds;f\right\rangle.$$

The procedure for taking the derivative of ϑ_s with respect to $\mathbf{r}$ and integrating over the volume is given in Appendix C. The result is an expression for the force on the CV rewritten as the force over each surface of the CV. For the x^+ face, for example, this is

$$\int_{S_x^+}\boldsymbol{\sigma}\cdot d\mathbf{S}_{S_x^+}=-\frac{1}{4}\sum_{i,j}^{N}\langle\mathbf{f}_{ij}[\operatorname{sgn}(x^+-x_j)-\operatorname{sgn}(x^+-x_i)]S_{xij}^+;f\rangle.$$

The combination of the signum functions and the S_{xij}^+ term specifies when the point of intersection of the line between i and j is located on the x^+ surface of the cube (see Appendix C). Corresponding expressions for the y and z faces are defined by $S_{\alpha ij}^{\pm}$ when $\alpha=\{y,z\}$, respectively.

The full expression for the MOP pressure tensor, which includes the kinetic part given by Eq. (26), is obtained by assuming a uniform pressure over the x^+ surface,

$$\int_{S_x^+}\boldsymbol{\Pi}\cdot d\mathbf{S}_x^+=[\boldsymbol{\kappa}-\boldsymbol{\sigma}]\cdot\mathbf{n}_x^+\Delta A_x^+\equiv[\mathbf{K}_x^+-\boldsymbol{T}_x^+]\Delta A_x^+=\mathbf{P}_x^+\Delta A_x^+,\qquad(44)$$

where $\mathbf{n}_x^+$ is a unit vector aligned along the x coordinate axis, $\mathbf{n}_x^+=[+1,0,0]$, $\boldsymbol{T}_x^+$ is the configurational stress (traction), and $\mathbf{P}_x^+$ the total pressure tensor acting on a plane. Hence,

$$\mathbf{P}_x^+=\frac{1}{\Delta A_x^+}\sum_{i=1}^{N}\left\langle\frac{\overline{\mathbf{p}}_i\overline{p}_{ix}}{m_i}\delta(x_i-x^+)S_{xi}^+;f\right\rangle+\frac{1}{4\Delta A_x^+}\sum_{i,j}^{N}\langle\mathbf{f}_{ij}[\operatorname{sgn}(x^+-x_j)-\operatorname{sgn}(x^+-x_i)]S_{xij}^+;f\rangle,\qquad(45)$$

where the peculiar momentum, $\overline{\mathbf{p}}_i$ has been used as in Todd *et al.* [13]. If the x^+ surface area covers the entire domain [$S_{xij}^+=1$ in Eq. (45)], the MOP formulation of the pressure is recovered [13].

The extent of the surface is defined through S_{xij}^+, in Eq. (45) which is the localized form of the pressure tensor considered by Han and Lee [14] applied to the six cubic faces. For a cube in space, each face has three components of stress, which results in 18 independent components over the total control surface. The quantity

$$dS_{\alpha ij}\equiv\tfrac{1}{2}[\operatorname{sgn}(r_\alpha^+-r_{\alpha j})-\operatorname{sgn}(r_\alpha^+-r_{\alpha i})]S_{\alpha ij}^+-\tfrac{1}{2}[\operatorname{sgn}(r_\alpha^--r_{\alpha j})-\operatorname{sgn}(r_\alpha^--r_{\alpha i})]S_{\alpha ij}^-,$$

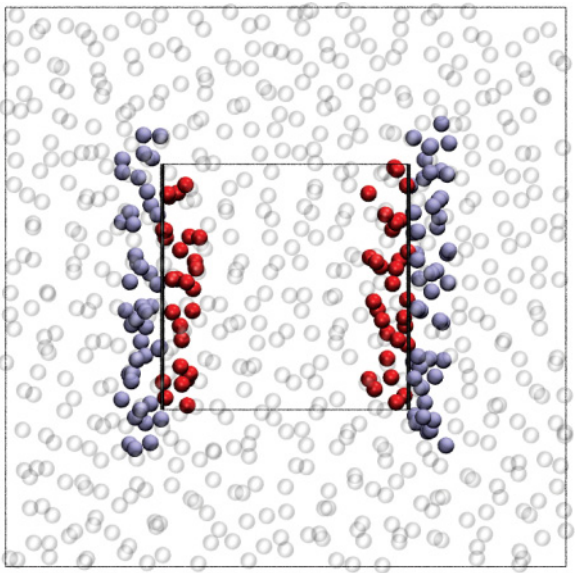

FIG. 4. (Color online) Representation of those molecules selected through dS_{xij} in Eq. (46) with molecules i on the side of the surface inside the CV (red) and molecules j on the outside (blue). The CV is the inner square on the figure.

selects the force contributions across the two opposite faces; similar notation to the surface molecular flux, $d\mathbf{S}_{ij}=d\mathbf{S}_{ij}^+-d\mathbf{S}_{ij}^-$ [cf. Eq. (17)], is used. The case of the two x planes located on opposite sides of the cube is illustrated in Fig. 4.

Taking all surfaces of the cube into account yields the final form,

$$\begin{aligned}\sum_{\text{faces}}^{6}\int_{S_f}\boldsymbol{\sigma}\cdot d\mathbf{S}_f&=-\frac{1}{2}\sum_{i,j}^{N}\left\langle\mathbf{f}_{ij}\sum_{\alpha=1}^{3}dS_{\alpha ij};f\right\rangle\\&=-\frac{1}{2}\sum_{i,j}^{N}\langle\mathbf{f}_{ij}\tilde{\mathbf{n}}\cdot d\mathbf{S}_{ij};f\rangle\\&=\frac{1}{2}\sum_{i,j}^{N}\langle\boldsymbol{\varsigma}_{ij}\cdot d\mathbf{S}_{ij};f\rangle.\end{aligned}\qquad(46)$$

The vector $\tilde{\mathbf{n}}$, obtained in Appendix C, is unity in each direction. The tensor $\boldsymbol{\varsigma}_{ij}$ is defined, for notational convenience, to be the outer product of the intermolecular forces with $\tilde{\mathbf{n}}$,

$$\boldsymbol{\varsigma}_{ij}\equiv-\mathbf{f}_{ij}\tilde{\mathbf{n}}=-\mathbf{f}_{ij}[1\ \ 1\ \ 1]=-\begin{bmatrix}f_{xij}&f_{xij}&f_{xij}\\f_{yij}&f_{yij}&f_{yij}\\f_{zij}&f_{zij}&f_{zij}\end{bmatrix}.$$

In this form, the ϑ_{ij} function for all interactions over the cube's surface is expressed as the sum of six selection functions for each of the six faces, i.e., $\vartheta_{ij}=-\sum_{\alpha=1}^{3}dS_{\alpha ij}$.

4. *Relationship to the continuum*

The forces per unit area, or "tractions," acting over each face of the CV, are used in the definition of the Cauchy stress tensor at the continuum level. For the x^+ surface, the traction

vector is the sum of all forces acting over the surface,

$$\mathbf{T}_x^+ = -\frac{1}{4\Delta A_x^+}\sum_{i,j}^{N}\langle \mathbf{f}_{ij}[\mathrm{sgn}(x^+ - x_j) - \mathrm{sgn}(x^+ - x_i)]S_{xij}^+;f\rangle, \tag{47}$$

which satisfies the definition,

$$\mathbf{T}_x^\pm = \boldsymbol{\sigma}\cdot\mathbf{n}_x^\pm,$$

of the Cauchy traction [42]. A similar relationship can be written for both the kinetic and total pressures,

$$\boldsymbol{K}_x^\pm = \boldsymbol{\kappa}\cdot\mathbf{n}_x^\pm, \quad \mathbf{P}_x^\pm = \boldsymbol{\Pi}\cdot\mathbf{n}_x^\pm,$$

where $\mathbf{n}_x^\pm$ is a unit vector, $\mathbf{n}_x^\pm = [\pm 1 \;\; 0 \;\; 0]^T$.

The time evolution of the molecular momentum within a CV [Eq. (30)], can be expressed in a similar form to the Navier-Stokes equations of continuum fluid mechanics. Dividing both sides of Eq. (30) by the volume, the following form can be obtained; note that this step requires Eqs. (26), (45), and (47),

$$\frac{1}{\Delta V}\frac{\partial}{\partial t}\sum_{i=1}^{N}\langle p_{\alpha i}\vartheta_i;f\rangle + \frac{\{\rho u_\alpha u_\beta\}^+ - \{\rho u_\alpha u_\beta\}^-}{\Delta r_\beta} = -\frac{K_{\alpha\beta}^+ - K_{\alpha\beta}^-}{\Delta r_\beta} + \frac{T_{\alpha\beta}^+ - T_{\alpha\beta}^-}{\Delta r_\beta} + \frac{1}{\Delta V}\sum_{i=1}^{N}\left\langle f_{\alpha i_{\mathrm{ext}}}\vartheta_i;f\right\rangle, \tag{49}$$

where index notation has been used (e.g., $\mathbf{T}_x^\pm = T_{\alpha x}^\pm$) with the Einstein summation convention.

In the limit of zero volume, each expression would be similar to a term in the differential continuum equations (although the pressure term would be the divergence of a tensor and not the gradient of a scalar field as is common in fluid mechanics). The Cauchy stress tensor, $\boldsymbol{\sigma}$, is defined in the limit that the cube's volume tends to zero, so $\mathbf{T}^+$ and $\mathbf{T}^-$ are related by an infinitesimal difference. This is used in continuum mechanics to define the unique nine component Cauchy stress tensor, $d\boldsymbol{\sigma}/dx \equiv \lim_{\Delta x\to 0}[\mathbf{T}^+ + \mathbf{T}^-]/\Delta x$. This limit is shown in Appendix B to yield the Irving and Kirkwood [8] stress in terms of the Taylor expansion in Dirac δ functions.

Rather than defining the stress at a point, the tractions can be compared to their continuum counterparts in a fluid mechanics control volume or a solid mechanics finite elements (FE) method. Computational fluid dynamics (CFD) is commonly formulated using CV and in discrete simulations, finite volume [4]. Surface forces are ideal for coupling schemes between MD and CFD. Building on the pioneering work of O'Connell and Thompson [23], there are many MD to CFD coupling schemes—see e.g. the review paper by Mohamed and Mohamad [43]. More recent developments for coupling to fluctuating hydrodynamics are covered in a review by Delgado-Buscalioni [44]. A discussion of coupling schemes is outside the scope of this work; however, finite volume algorithms have been used extensively in coupling methods [31,32,45,46,51] together with equivalent control volumes defined in the molecular region. An advantage of the herein proposed molecular CV approach is that it ensures conservation laws are satisfied when exchanging fluxes over cell surfaces—an important requirement for accurate unsteady coupled simulations as outlined in the finite volume coupling of Delgado-Buscalioni and Coveney [45]. For solid coupling schemes [30], the principle of virtual work can be used with tractions on the element corners (the MD CV) to give the state of stress in the element [47],

$$\int_V \boldsymbol{\sigma}\cdot\nabla N_a dV = \oint_S N_a \mathbf{T} dS, \tag{50}$$

where N_a is a shape function which allows stress to be defined as a continuous function of position. It will be demonstrated numerically in the next section (Sec. IV) that the CV formulation is exactly conservative: The surface tractions and fluxes entirely define the stress within the volume. The tractions and stress in Eq. (50) are connected by the weak formulation and the form of the stress tensor results from the choice of shape function N_a.

D. Energy balance for a molecular CV

In this section, a mesoscopic expression for the time evolution of energy within a CV is derived. As for mass and momentum, the starting point is to integrate the energy at a point, given in Eq. (10), over the CV,

$$\int_V \rho(\mathbf{r},t)\mathcal{E}(\mathbf{r},t)dV = \sum_{i=1}^{N}\langle e_i\vartheta_i;f\rangle. \tag{51}$$

The time evolution within the CV is given using formula (12),

$$\frac{\partial}{\partial t}\int_V \rho(\mathbf{r},t)\mathcal{E}(\mathbf{r},t)dV = \frac{\partial}{\partial t}\sum_{i=1}^{N}\langle e_i\vartheta_i;f\rangle = \sum_{i=1}^{N}\left\langle \frac{\mathbf{p}_i}{m_i}\cdot\frac{\partial}{\partial\mathbf{r}_i}e_i\vartheta_i + \mathbf{F}_i\cdot\frac{\partial}{\partial\mathbf{p}_i}e_i\vartheta_i;f\right\rangle. \tag{52}$$

Evaluating the derivatives of the energy and $\mathcal{LCV}$ function results in

$$\frac{\partial}{\partial t}\sum_{i=1}^{N}\langle e_i\vartheta_i;f\rangle = -\frac{1}{2}\sum_{i,j}^{N}\left\langle\left[\frac{\mathbf{p}_i}{m_i}\cdot\mathbf{f}_{ij} + \frac{\mathbf{p}_j}{m_i}\cdot\mathbf{f}_{ji}\right]\vartheta_i;f\right\rangle - \sum_{i=1}^{N}\left\langle e_i\frac{\mathbf{p}_i}{m_i}\cdot d\mathbf{S}_i - \mathbf{F}_i\cdot\frac{\mathbf{p}_i}{m_i}\vartheta_i;f\right\rangle.$$

Using the definition of $\mathbf{F}_i$, Newton's third law and relabelling indices, the intermolecular force terms can be expressed in terms of the interactions over the CV surface, ϑ_{ij},

$$\frac{\partial}{\partial t}\sum_{i=1}^{N}\langle e_i\vartheta_i;f\rangle = -\sum_{i=1}^{N}\left\langle e_i\frac{\mathbf{p}_i}{m_i}\cdot d\mathbf{S}_i;f\right\rangle + \frac{1}{2}\sum_{i,j}^{N}\left\langle\frac{\mathbf{p}_i}{m_i}\cdot\mathbf{f}_{ij}\vartheta_{ij};f\right\rangle + \sum_{i=1}^{N}\left\langle\frac{\mathbf{p}_i}{m_i}\cdot\mathbf{f}_{i_{\mathrm{ext}}}\vartheta_i;f\right\rangle.$$

The right-hand side of this equation is equated to the right-hand side of the continuum energy Eq. (4),

$$\overbrace{-\oint_S \rho\mathcal{E}\boldsymbol{u}\cdot d\mathbf{S}}^{\text{energy flux}} - \overbrace{\oint_S \mathbf{q}\cdot d\mathbf{S}}^{\text{heat flux}} - \overbrace{\oint_S \boldsymbol{\Pi}\cdot\boldsymbol{u}\cdot d\mathbf{S}}^{\text{pressure heating}} = -\sum_{i=1}^{N}\left\langle e_i\frac{\mathbf{p}_i}{m_i}\cdot d\mathbf{S}_i;f\right\rangle + \frac{1}{2}\sum_{i,j}^{N}\left\langle\frac{\mathbf{p}_i}{m_i}\cdot\boldsymbol{\varsigma}_{ij}\cdot d\mathbf{S}_{ij};f\right\rangle, \quad (53)$$

where the energy due to the external (body) forces is neglected. The $\mathbf{f}_{ij}\vartheta_{ij}$ has been re-expressed in terms of surface tractions, $\boldsymbol{\varsigma}_{ij}\cdot d\mathbf{S}_{ij}$, using the analysis of the previous section. In its current form, the microscopic equation does not delineate between the contribution due to energy flux, heat flux, and pressure heating. To achieve this division, the notion of the peculiar momentum at the molecular location, $\boldsymbol{u}(\mathbf{r}_i)$, is used together with the velocity at the CV surfaces, $\boldsymbol{u}(\mathbf{r}^{\pm})$, following a process similar to that of Evans and Morriss [7].

IV. IMPLEMENTATION

In this section, the CV equation for mass, momentum, and energy balance, Eqs. (22), (30), and (53), will be proved to apply and demonstrated numerically for a microscopic system undergoing a single trajectory through phase space.

A. The microscopic system

Consider a single trajectory of a set of molecules through phase space, defined in terms of their time dependent coordinates $\mathbf{r}_i$ and momentum $\mathbf{p}_i$. The $\mathcal{LCV}$ function depends on molecular coordinates, the location of the center of the cube, $\mathbf{r}$, and its side length, $\Delta\mathbf{r}$, i.e., $\vartheta_i \equiv \vartheta_i(\mathbf{r}_i(t),\mathbf{r},\Delta\mathbf{r})$. The time evolution of the mass within the molecular control volume is given by

$$\frac{d}{dt}\sum_{i=1}^{N} m_i\vartheta_i(\mathbf{r}_i(t),\mathbf{r},\Delta\mathbf{r}) = \sum_{i=1}^{N} m_i\frac{\partial\vartheta_i}{\partial t} = \sum_{i=1}^{N} m_i\frac{d\mathbf{r}_i}{dt}\cdot\frac{\partial\vartheta_i}{\partial\mathbf{r}_i} = -\sum_{i=1}^{N}\mathbf{p}_i\cdot d\mathbf{S}_i, \quad (54)$$

using $\mathbf{p}_i = m_i d\mathbf{r}_i/dt$. The time evolution of momentum in the molecular control volume is

$$\frac{\partial}{\partial t}\sum_{i=1}^{N}\mathbf{p}_i(t)\vartheta_i(\mathbf{r}_i(t),\mathbf{r},\Delta\mathbf{r}) = \sum_{i=1}^{N}\left[\mathbf{p}_i\frac{\partial\vartheta_i}{\partial t} + \frac{d\mathbf{p}_i}{dt}\vartheta_i\right] = \sum_{i=1}^{N}\left[\mathbf{p}_i\frac{d\mathbf{r}_i}{dt}\cdot\frac{\partial\vartheta_i}{\partial\mathbf{r}_i} + \frac{d\mathbf{p}_i}{dt}\vartheta_i\right].$$

As $d\mathbf{p}_i/dt = \mathbf{F}_i$, then,

$$\frac{\partial}{\partial t}\sum_{i=1}^{N}\mathbf{p}_i\vartheta_i = \sum_{i=1}^{N}\left[-\frac{\mathbf{p}_i\mathbf{p}_i}{m_i}\cdot d\mathbf{S}_i + \mathbf{F}_i\vartheta_i\right] = -\sum_{i=1}^{N}\frac{\mathbf{p}_i\mathbf{p}_i}{m_i}\cdot d\mathbf{S}_i + \frac{1}{2}\sum_{i,j}^{N}\mathbf{f}_{ij}\vartheta_{ij} + \sum_{i=1}^{N}\mathbf{f}_{i_{\text{ext}}}\vartheta_i, \quad (55)$$

where the total force on molecule i has been decomposed into surface and "external" or body terms. The time evolution of energy in a molecular control volume is obtained by evaluating

$$\frac{\partial}{\partial t}\sum_{i=1}^{N} e_i\vartheta_i = \sum_{i=1}^{N}\left[e_i\frac{\partial\vartheta_i}{\partial t} + \frac{\partial e_i}{\partial t}\vartheta_i\right] = -\sum_{i=1}^{N} e_i\frac{\mathbf{p}_i}{m_i}\cdot d\mathbf{S}_i + \sum_{i=1}^{N}\frac{\dot{\mathbf{p}}_i\cdot\mathbf{p}_i}{m_i}\vartheta_i - \frac{1}{2}\sum_{i,j}^{N}\left[\frac{\mathbf{p}_i}{m_i}\cdot\mathbf{f}_{ij} + \frac{\mathbf{p}_j}{m_j}\cdot\mathbf{f}_{ji}\right]\vartheta_i$$

using $d\mathbf{p}_i/dt = \mathbf{F}_i$ and the decomposition of forces. The manipulation proceeds as in the mesoscopic system to yield

$$\frac{\partial}{\partial t}\sum_{i=1}^{N} e_i\vartheta_i = -\sum_{i=1}^{N} e_i\frac{\mathbf{p}_i}{m_i}\cdot d\mathbf{S}_i + \frac{1}{2}\sum_{i,j}^{N}\frac{\mathbf{p}_i}{m_i}\cdot\mathbf{f}_{ij}\vartheta_{ij} + \sum_{i=1}^{N}\frac{\mathbf{p}_i}{m_i}\cdot\mathbf{f}_{i_{\text{ext}}}\vartheta_i. \quad (56)$$

The average of many such trajectories defined through Eqs. (54)–(56) gives the mesoscopic expressions in Eqs. (22), (30), and (53), respectively. In the next subsection, the time integral of the single trajectory is considered.

B. Time integration of the microscopic CV equations

Integration of Eqs. (54)–(56) over the time interval $[0,\tau]$ enables these equations to be used in a molecular simulation. For the conservation of mass term,

$$\sum_{i=1}^{N} m_i\left[\vartheta_i(\tau) - \vartheta_i(0)\right] = -\int_0^{\tau}\sum_{i=1}^{N}\mathbf{p}_i\cdot d\mathbf{S}_i dt. \quad (57)$$

The surface crossing term, $d\mathbf{S}_i$, defined in Eq. (16), involves a Dirac δ function and therefore cannot be evaluated directly. Over the time interval $[0,\tau]$, molecule i passes through a given x position at times, $t_{xi,k}$, where $k = 1,2,\ldots,N_{t_x}$ [48]. The positional Dirac δ can be expressed as

$$\delta[x_i(t) - x] = \sum_{k=1}^{N_{t_x}}\frac{\delta(t - t_{xi,k})}{|\dot{x}_i(t_{xi,k})|}, \quad (58)$$

where $|\dot{x}_i(t_{xi,k})|$ is the magnitude of the velocity in the x direction at time $t_{xi,k}$. Equation (58) is used to rewrite $d\mathbf{S}_i$ in Eq. (57) in the form

$$dS_{\alpha i,k} \equiv [\text{sgn}(t^+_{\alpha i,k} - \tau) - \text{sgn}(t^+_{\alpha i,k} - 0)]S^+_{\alpha i,k}(t^+_{\alpha i,k}) - [\text{sgn}(t^-_{\alpha i,k} - \tau) - \text{sgn}(t^-_{\alpha i,k} - 0)]S^-_{\alpha i,k}(t^-_{\alpha i,k}), \quad (59)$$

where $\alpha = \{x,y,z\}$ and the fluxes are evaluated at times $t^+_{\alpha i,k}$ and $t^-_{\alpha i,k}$ for the right and left surfaces of the cube, respectively. Using the above expression, the time integral in Eq. (57) can be expressed as the sum of all molecule crossings,

$N_t = N_{t_x} + N_{t_y} + N_{t_z}$, over the cube's faces,

$$\overbrace{\sum_{i=1}^{N} m_i \left[\vartheta_i(\tau) - \vartheta_i(0)\right]}^{\text{Accumulation}} = \underbrace{-\sum_{i=1}^{N}\sum_{k=1}^{N_t} m_i \sum_{\alpha=1}^{3} \frac{p_{\alpha i}}{|p_{\alpha i}|} dS_{\alpha i,k}}_{\text{Advection}} . \quad (60)$$

In other words, the mass in a CV at time $t = \tau$ minus its initial value at $t = 0$ is the sum of all molecules that cross its surfaces during the time interval.

The momentum balance equation, Eq. (55), can also be written in time-integrated form,

$$\sum_{i=1}^{N} \left[\mathbf{p}_i(\tau)\vartheta_i(\tau) - \mathbf{p}_i(0)\vartheta_i(0)\right] = -\int_0^\tau \left[\sum_{i=1}^{N} \frac{\mathbf{p}_i\mathbf{p}_i}{m_i} \cdot d\mathbf{S}_i - \frac{1}{2}\sum_{i,j}^{N} \mathbf{f}_{ij}\vartheta_{ij} - \sum_{i=1}^{N} \mathbf{f}_{i_{\text{ext}}}\vartheta_i\right] dt,$$

and using identity (59),

$$\overbrace{\sum_{i=1}^{N} \left[\mathbf{p}_i(\tau)\vartheta_i(\tau) - \mathbf{p}_i(0)\vartheta_i(0)\right]}^{\text{Accumulation}} + \overbrace{\sum_{i=1}^{N}\sum_{k=1}^{N_t} \mathbf{p}_i \sum_{\alpha=1}^{3} \frac{p_{\alpha i}}{|p_{\alpha i}|} dS_{\alpha i,k}}^{\text{Advection}} = \underbrace{\sum_{i,j}^{N} \int_0^\tau \mathbf{f}_{ij}(t)\vartheta_{ij}(t)dt + \sum_{i=1}^{N} \int_0^\tau \mathbf{f}_{i_{\text{ext}}}(t)\vartheta_i(t)dt}_{\text{Forcing}} . \quad (61)$$

The integral of the forcing term can be rewritten as the sum

$$\int_0^\tau \mathbf{f}_{ij}(t)\vartheta_{ij}(t)dt \approx \Delta t \sum_{n=1}^{N_\tau} \mathbf{f}_{ij}(t_n)\,\vartheta_{ij}(t_n),$$

where N_τ is the number time steps. Equation (61) can be rearranged as follows:

$$\sum_{i=1}^{N} \frac{p_{\alpha i}(\tau)\vartheta_i(\tau) - p_{\alpha i}(0)\vartheta_i(0)}{\tau \Delta V} + \frac{\{\overline{\rho u_\alpha u_\beta}\}^+ - \{\overline{\rho u_\alpha u_\beta}\}^-}{\Delta r_\beta} = -\frac{\overline{K}^+_{\alpha\beta} - \overline{K}^-_{\alpha\beta}}{\Delta r_\beta} + \frac{\overline{T}^+_{\alpha\beta} - \overline{T}^-_{\alpha\beta}}{\Delta r_\beta} + \frac{1}{N_\tau \Delta V}\sum_{i=1}^{N}\sum_{n=1}^{N_\tau} f_{\alpha i_{\text{ext}}}(t_n)\vartheta_i(t_n), \quad (62)$$

where the overbar denotes the time average. The time-averaged traction in Eq. (62) is given by

$$\overline{T}^{\pm}_{\alpha\beta} = -\frac{1}{N_\tau}\frac{1}{4\Delta A_\beta}\sum_{i,j}^{N}\sum_{n=1}^{N_\tau} \mathbf{f}_{\alpha ij}(t_n) dS^{\pm}_{\beta ij}(t_n).$$

The time-averaged kinetic surface pressure in Eq. (62) is

$$\overline{K}^{\pm}_{\alpha\beta} = \frac{1}{\tau}\frac{1}{2\Delta A_\beta}\sum_{i=1}^{N}\sum_{k=1}^{N_t} \frac{p_{\alpha i}(t_k)p_{\beta i}(t_k)}{|p_{\beta i}(t_k)|} dS^{\pm}_{\beta i,k}(t_k) - \{\overline{\rho u_\alpha u_\beta}\}^{\pm}.$$

Equation (62) demonstrates that the time average of the fluxes, stresses, and body forces on a CV during the interval 0 to τ completely determines the change in momentum within the CV for a single trajectory of the system through phase space (i.e., an MD simulation). The time evolution of the microscopic system, Eq. (62), can also be obtained directly by evaluating the derivatives of the mesoscopic expression (49) and invoking the ergodic hypothesis, hence, replacing $\langle \alpha; f \rangle$ with $\frac{1}{\tau}\int_0^\tau \alpha dt$. The use of the ergodic hypothesis is justified provided that the time interval, τ, is sufficient to ensure phase space is adequately sampled.

Finally, there are no new techniques required to integrate the energy Eq. (56),

$$\sum_{i=1}^{N} \left[e_i(\tau)\vartheta_i(\tau) - e_i(0)\vartheta_i(0)\right] = -\int_0^\tau \left[\sum_{i=1}^{N} e_i \frac{\mathbf{p}_i}{m_i} \cdot d\mathbf{S}_i - \frac{1}{2}\sum_{i,j}^{N} \frac{\mathbf{p}_i}{m_i} \cdot \mathbf{f}_{ij}\vartheta_{ij}\right] dt \quad (63)$$

which gives the final form, written without external forcing,

$$\overbrace{\sum_{i=1}^{N} \left[e_i(\tau)\vartheta_i(\tau) - e_i(0)\vartheta_i(0)\right]}^{\text{Accumulation}} + \overbrace{\sum_{i=1}^{N}\sum_{k=1}^{N_t} e_i \sum_{\alpha=1}^{3} \frac{p_{\alpha i}}{|p_{\alpha i}|} dS_{\alpha i,k}}^{\text{Advection}} = \underbrace{\frac{1}{2}\sum_{i,j}^{N} \int_0^\tau \frac{\mathbf{p}_i(t)}{m_i} \cdot \mathbf{f}_{ij}(t)\vartheta_{ij}(t)dt}_{\text{Forcing}} . \quad (64)$$

As in the momentum balance equation, the integral of the forcing term can be approximated by the sum

$$\int_0^\tau \frac{\mathbf{p}_i(t)}{m_i} \cdot \mathbf{f}_{ij}(t)\vartheta_{ij}(t)dt \approx \Delta t \sum_{n=1}^{N_\tau} \frac{\mathbf{p}_i(t_n)}{m_i} \cdot \mathbf{f}_{ij}(t_n)\,\vartheta_{ij}(t_n),$$

where N_τ is the number time steps.

In the next section, the elements Accumulation, Advection, and Forcing in the above equations are computed individually in an MD simulation to confirm Eqs. (60), (61), and (64) numerically.

C. Results and discussion

Molecular dynamics (MD) simulations in 3D are used in this section to validate numerically and explore the statistical convergence of the CV formalism for three test cases. The first investigation was to confirm numerically the conservation properties of an arbitrary control volume. The second simulation compares the value of the scalar pressure obtained from the molecular CV formulation with that of the virial expression for an equilibrium system in a periodic domain. The final test is a nonequilibrium molecular dynamics (NEMD) simulation of the start-up of Couette flow initiated by translating the top wall in a slit channel geometry. The NEMD system is analyzed using the CV expressions Eqs. (60), (61), and (64), and the shear pressure was computed by the VA and CV routes. Newton's equations of motion were integrated using the half-step leap-frog Verlet algorithm [49]. The repulsive Lennard-Jones (LJ) or Weeks-Chandler-Anderson (WCA)

potential [50],

$$\Phi(r_{ij}) = 4\epsilon\left[\left(\frac{\ell}{r_{ij}}\right)^{12} - \left(\frac{\ell}{r_{ij}}\right)^{6}\right] + \epsilon, \quad r_{ij} \leqslant r_c, \qquad (65)$$

was used for the molecular interactions, which is the Lennard-Jones potential shifted upward by ϵ and truncated at the minimum in the potential, $r_{ij} = r_c \equiv 2^{1/6}\ell$. The potential is zero for $r_{ij} > r_c$. The energy scale is set by ϵ, the length scale by ℓ, and molecular mass by m. The results reported here are given in terms of ℓ, ϵ, and m. A time step of 0.005 was used for all simulations. The domain size in the first two simulations was 13.68, which contained $N = 2048$ molecules, the density was $\rho = 0.8$, and the reduced temperature was set to an initial value of $T = 1.0$. Test cases 1 and 2 described below are for equilibrium systems and, therefore, did not require thermostatting. Case 3 is for a nonequilibrium system and required removal of generated heat, which was achieved by thermostatting the wall atoms only.

1. Case 1

In case 1, the periodic domain simulates a constant energy ensemble. The separate terms of the integrated mass, momentum, and energy equations given in Eqs. (60), (61), and (64) were evaluated numerically for several sizes of CV. The mass conservation can readily be shown to be satisfied as it simply requires tracking the number of molecules in the CV. The momentum and energy balance equations are conveniently checked for compliance at all times by evaluating the residual quantity,

$$\text{Residual} = \text{Accumulation} - \text{Forcing} + \text{Advection}, \qquad (66)$$

which must be equal to zero at all times for the CV equations to be satisfied. This was demonstrated to be the case, as may be seen in Figs. 5(a) and 5(b), for a cubic CV of side length 1.52 in the absence of body forces. The evolution of momentum inside the CV is shown numerically to be exactly equal to the integral of the surface forces until a molecule crosses the CV boundary. Such events give rise to a momentum flux contribution which appears as a spike in the Advection and Accumulation terms, as is evident in Fig. 5(a). The residual nonetheless remains identically zero (to machine precision) at all times. The energy conservation is also displayed in Fig. 5(b). The average error over the period of the simulation (100 MD time units) was less than 1%, where the average error is defined as the ratio of the mean |Residual| to the mean |Accumulation| over the simulation. The error is attributed to the use of the leapfrog integration scheme, a conclusion supported by the linear decrease in error as time step $\Delta t \to 0$.

2. Case 2

As in case 1, the same periodic domain is used in case 2 to simulate a constant energy ensemble. The objective of this exercise is to show that the average of the virial formula for the scalar pressure, Π_{vir}, applicable to an equilibrium periodic system,

$$\Pi_{\text{vir}} = \frac{1}{3V}\sum_{i=1}^{N}\left\langle \frac{\overline{\mathbf{p}}_i \cdot \overline{\mathbf{p}}_i}{m_i} + \frac{1}{2}\sum_{i\neq j}^{N}\mathbf{f}_{ij}\cdot\mathbf{r}_{ij}; f\right\rangle, \qquad (67)$$

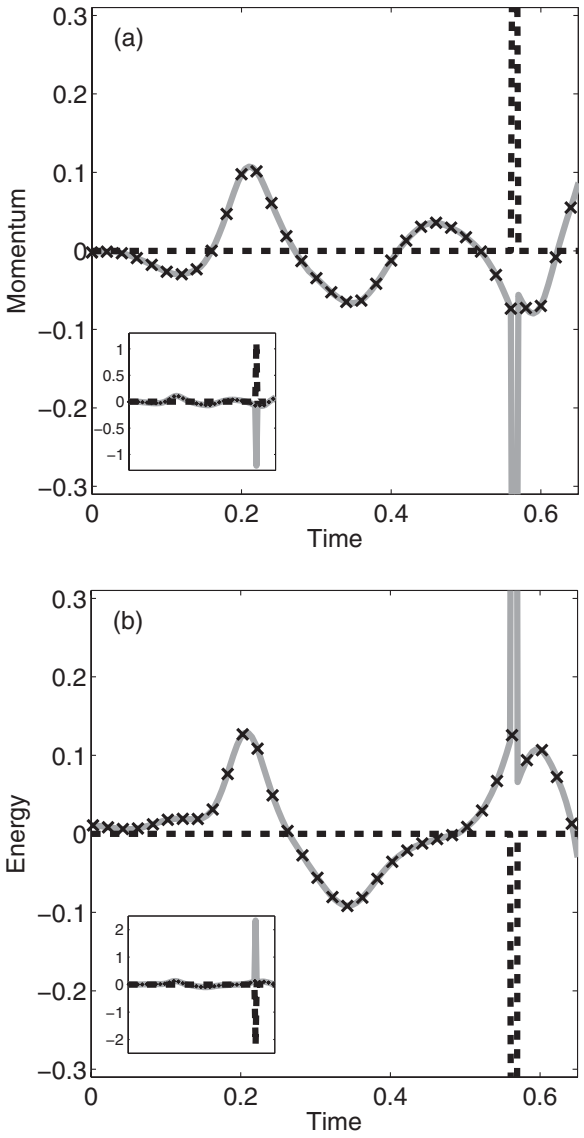

FIG. 5. The various components in Eq. (66), "Accumulation" (—), the time integral of the surface force, "Forcing" (×), and the momentum flux term, "Advection" (- - -), are shown. "Forcing" symbols are shown every fourth time step for clarity and the insert shows the full ordinate scale over the same time interval on the abscissa. From top to bottom, (a) momentum control volume and (b) energy control volume.

arises from the intermolecular interactions across the periodic boundaries [12]. The CV formula for the scalar pressure is

$$\Pi_{\text{CV}} = \tfrac{1}{6}(P^{+}_{xx} + P^{-}_{xx} + P^{+}_{yy} + P^{-}_{yy} + P^{+}_{zz} + P^{-}_{zz}), \qquad (68)$$

where the $P^{\pm}_{\alpha\alpha}$ normal pressure is defined in Eq. (45) and includes both the kinetic and configurational components on each surface. Both routes involve the pair forces, f_{ij}. However, the CV expression which uses MOP counts only those pair forces which cross a plane while VA (virial) sums $f_{ij}r_{ij}$ over the whole volume. It is, therefore, expected that there would be differences between the two methods at short times, converging at long times. A control volume the same size as the periodic box was taken. The time-averaged control volume, (Π_{CV}) and virial (Π_{vir}) pressure values are shown in Fig. 6 to

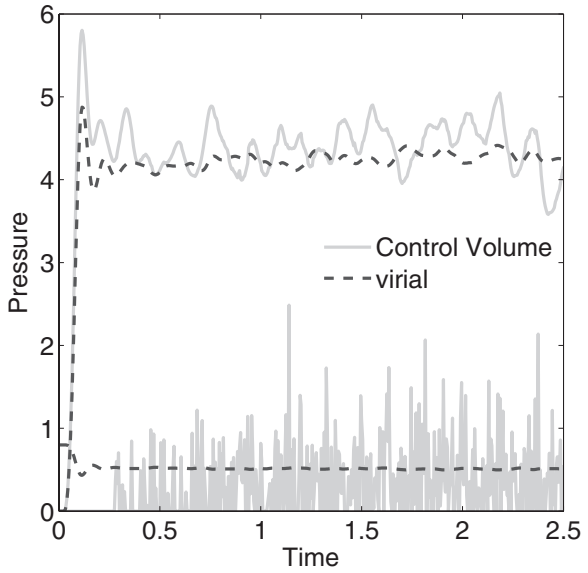

FIG. 6. $\Pi_{\rm vir}$ and $\Pi_{\rm CV}$ from Eqs. (67) and (68), respectively. The configurational and kinetic pressures are separated with configurational values typically having greater magnitudes (∼4.0) than kinetic (∼0.6). Continuous lines are control volume pressures and dotted lines are virial pressure.

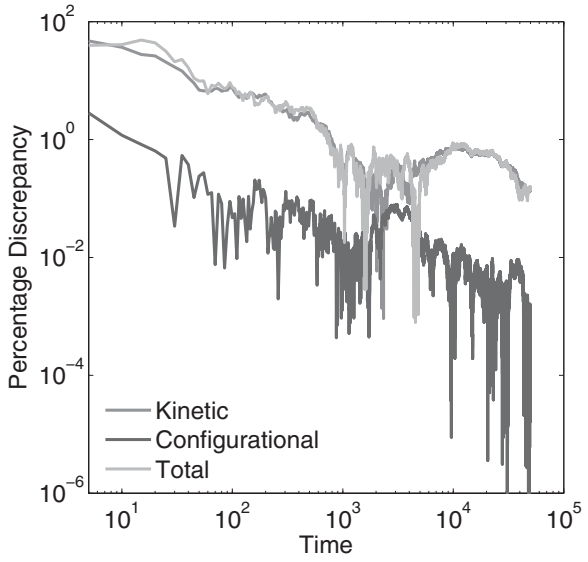

FIG. 7. The percentage relative difference between the virial and control volume time-accumulated scalar pressures (PD defined in the text). Values for the kinetic, configurational, and total PD are shown.

converge toward the same value with increasing time. The simulation was started from an FCC lattice with a short-range potential (WCA) so the initial configurational stress was zero. It is the evolution of the pressure from this initial state that is compared in Fig. 6. The virial kinetic pressure makes use of the instantaneous values of the domain molecule's velocities at every time step. In contrast, the CV kinetic part of the pressure is due to molecular surface crossings only, which may explain its slower convergence to the limiting value than the kinetic part of the virial expression. To quantify this difference in convergence for the two measures of the pressure, the standard deviation, SD(x), is evaluated, ensuring decorrelation [51] using block averaging [50]. For the kinetic virial, SD($\kappa_{\rm vir}$) = 0.0056, and configurational, SD($\sigma_{\rm vir}$) = 0.0619. For the kinetic CV pressure, SD($\kappa_{\rm CV}$) = 0.4549 and the configurational SD($\sigma_{\rm CV}$) = 0.2901. The CV pressure, which makes use of the MOP formula, would, therefore, require more samples to converge to a steady-state value. However, the MOP pressures are generally more efficient to calculate than the VA. More usefully, from an evaluation of only the interactions over the outer CV surface, the pressure in a volume of arbitrary size can be determined.

Figure 7 is a log-log plot of the percentage discrepancy (PD) between the two (PD = $[100 \times |\Pi_{\rm CV} - \Pi_{\rm vir}|/\Pi_{\rm vir}]$). After 10 million time steps or a reduced time of 5×10^4, the percentage discrepancy in the configurational part has decreased to 0.01% and the kinetic part of the pressure matches the virial (and kinetic theory) to within 0.1%. The total pressure value agrees to within 0.1% at the end of this averaging period. The simulation average temperature was 0.65, and the kinetic part of the CV pressure was statistically the same as the kinetic theory formula prediction, $\kappa_{\rm CV} = \rho k_B T = 0.52$ [50]. The VA formula for the pressure in a volume the size of the domain is, by definition, formally the same as that of the virial pressure.

The next test case compares the CV and VA formulas for the shear stress in a system out of equilibrium.

3. Case 3

In this simulation study, Couette flow was simulated by entraining a model liquid between two solid walls. The top wall was set in translational motion parallel to the bottom (stationary) wall and the evolution of the velocity profile toward the steady-state Couette flow limit was followed. The velocity profile, and the derived CV and VA shear stresses are compared with the analytical solution of the unsteady diffusion equation. Four layers of tethered molecules were used to represent each wall, with the top wall given a sliding velocity of, $U_0 = 1.0$ at the start of the simulation, time $t = 0$. The temperature of both walls was controlled by applying the Nosé-Hoover (NH) thermostat to the wall atoms [52]. The two walls were thermostatted separately, and the equations of motion of the wall atoms were

$$\dot{\mathbf{r}}_i = \frac{\overline{\mathbf{p}}_i}{m_i} + U_0 \mathbf{n}_x^+, \tag{69a}$$

$$\dot{\overline{\mathbf{p}}}_i = \mathbf{F}_i + \mathbf{f}_{i_{\rm ext}} - \xi \overline{\mathbf{p}}_i, \tag{69b}$$

$$\mathbf{f}_{i_{\rm ext}} = \mathbf{r}_{i_0} \left(4k_4 r_{i_0}^2 + 6k_6 r_{i_0}^4\right), \tag{69c}$$

$$\dot{\xi} = \frac{1}{Q_\xi} \left[\sum_{n=1}^{N} \frac{\overline{\mathbf{p}}_n \cdot \overline{\mathbf{p}}_n}{m_n} - 3T_0 \right], \tag{69d}$$

where $\mathbf{n}_x^+$ is a unit vector in the x direction, $m_n \equiv m$, and $\mathbf{f}_{i_{\rm ext}}$ is the tethered atom force, using the formula of Petravic and Harrowell [53] ($k_4 = 5 \times 10^3$ and $k_6 = 5 \times 10^6$). The vector, $\mathbf{r}_{i_0} = \mathbf{r}_i - \mathbf{r}_0$, is the displacement of the tethered atom, i, from its lattice site coordinate, $\mathbf{r}_0$. The Nosé-Hoover thermostat dynamical variable is denoted by ξ, $T_0 = 1.0$ is the target temperature of the wall, and the effective time constant or damping coefficient, in Eq. (69d), was given the value $Q_\xi = N\Delta t$. The simulation was carried out for a cubic domain of sidelength 27.40, of which the fluid region extent was

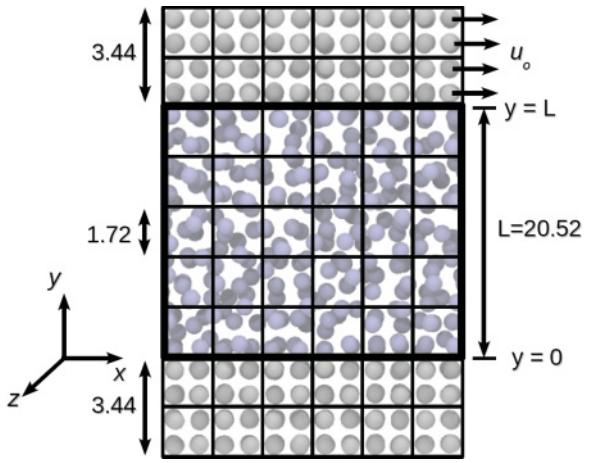

FIG. 8. (Color online) Schematic diagram of the NEMD simulation geometry consisting of a sliding top wall and stationary bottom wall, both composed of tethered atoms. The simulation domain contained a lattice of contiguous CV used for pressure averaging (shown by the small boxes) while the thicker line denotes a single CV containing the entire liquid region.

20.52 in the y direction. Periodic boundaries were used in the streamwise (x) and spanwise (z) directions. The results presented are the average of eight simulation trajectories starting with a different set of initial atom velocities. The lattice contained 16 384 molecules and was at a density of $\rho = 0.8$. The molecular simulation domain was subdivided into 4096 (16^3) control volumes, and the average velocity and shear stress was determined in each of them. A larger single CV encompassing all of the liquid region of the domain, shown bounded by the thick line in Fig. 8, was also considered.

The continuum solution for this configuration is considered now. Between two plates, there are no body forces and the flow eventually becomes fully developed, [54] so Eq. (2) can be simplified, and after applying the divergence theorem from Eq. (5) it becomes,

$$\frac{\partial}{\partial t}\int_V \rho \boldsymbol{u} dV = -\int_V \boldsymbol{\nabla}\cdot\boldsymbol{\Pi} dV,$$

which is valid for any arbitrary volume in the domain and must be valid at any point for a continuum. The shear pressure in the fluid, $\Pi_{xy}(y)$, drives the time evolution of the flow,

$$\frac{\partial \rho u_x}{\partial t} = -\frac{\partial \Pi_{xy}}{\partial y}.$$

For a Newtonian liquid with viscosity, μ, [54],

$$\Pi_{xy} = -\mu\frac{\partial u_x}{\partial y}, \tag{70}$$

which gives the 1D diffusion equation,

$$\frac{\partial u_x}{\partial t} = \frac{\mu}{\rho}\frac{\partial^2 u_x}{\partial y^2}, \tag{71}$$

assuming the liquid to be incompressible. This can be solved for the boundary conditions,

$$u_x(0,t) = 0 \quad u_x(L,t) = U_0 \quad u_x(y,0) = 0,$$

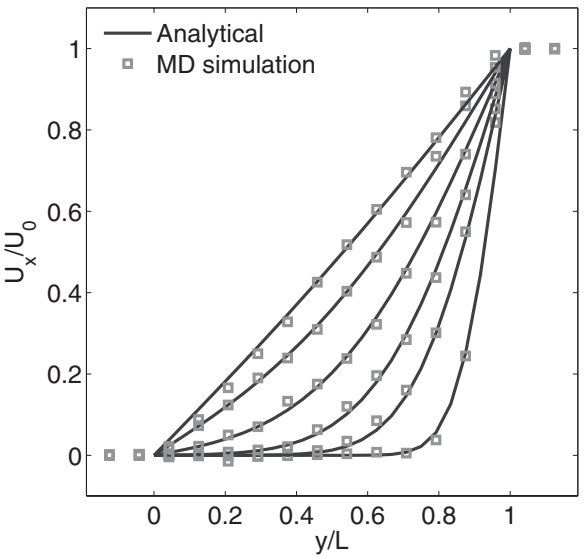

FIG. 9. The y dependence of the streaming velocity profile at times $t = 2^n$ for $n = 0,2,3,4,5,6$ from right to left. The squares are the NEMD CV data values and the analytical solution to the continuum equations of Eq. (72) is given at the same six times as continuous curves.

where the bottom and top wall-liquid boundaries are at $y = 0$ and $y = L$, respectively. The Fourier series solution of these equations with inhomogeneous boundary conditions [55] is

$$u_x(y,t) = \begin{cases} U_0 & y = L \\ \sum_{n=1}^{\infty} u_n(t)\sin\left(\frac{n\pi y}{L}\right) & 0 < y < L \\ 0 & y = 0 \end{cases}, \tag{72}$$

where $\lambda_n = (n\pi/L)^2$ and $u_n(t)$ is given by

$$u_n(t) = \frac{2U_0(-1)^n}{n\pi}\left[\exp\left(-\frac{\lambda_n \mu t}{\rho}\right) - 1\right].$$

The velocity profile resolved at the control volume level is compared with the continuum solution in Fig. 9. There were 16 cubic NEMD CV of side length 1.72 spanning the system in the y direction, with each data point on the figure being derived from a local time average of 0.5 time units. The analytic continuum solution was evaluated numerically from Eq. (72) with $n = 1000$ and $\mu = 1.6$, the latter a literature value for the WCA fluid shear viscosity at $\rho = 0.8$ and $T = 1.0$ [56]. There is mostly very good agreement between the analytic and NEMD velocity profiles at all times, although some effect of the stacking of molecules near the two walls can be seen in a slight blunting of the fluid velocity profile very close to the tethered walls (located by the horizontal two squares on the far left and right of the figure), which is an aspect of the molecular system that the continuum treatment is not capable of reproducing.

The VA and CV shear pressure, given by Eqs. (43) and (45), are compared at time $t = 10$ in Fig. 10. The comparison is for a single simulation trajectory resolved into 16 cubic volumes of size 1.72 in the y direction, with averaging in the x and z directions and over 0.5 in reduced time. The figure shows the shear pressure on the faces of the CV. Inside the CV, the pressure was assumed to vary linearly, and the value at the

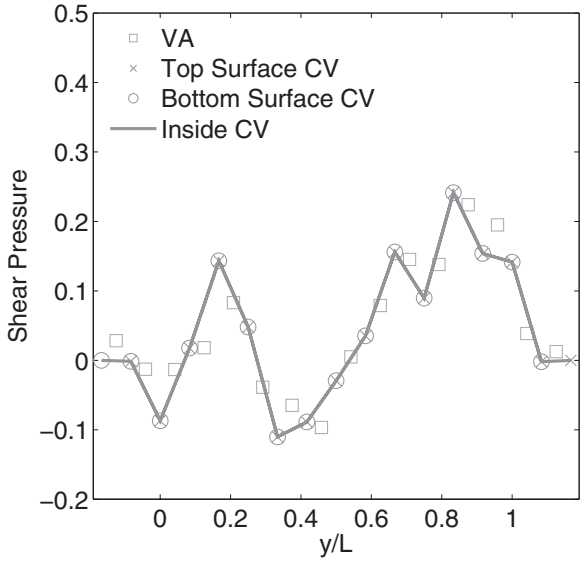

FIG. 10. The y dependence of the shear pressure at $t = 10$, averaged over 100 time steps and for a single simulation trajectory. The VA value from Eq. (43) are the squares. The CV surface traction from Eq. (45) is indicated by $\times$ and $\circ$ for the top and bottom surfaces, respectively. The solid gray line displays the resulting pressure field using Eq. (50) with linear shape functions.

midpoint is shown to be comparable to the VA-determined value. Figure 10 shows that there is good agreement between the VA and CV approaches. Note that the CV pressure is effectively the MOP formula applied to the faces of the cube and, hence, this case study demonstrates a consistency between MOP and VA. We have shown previously that this is true for the special case of an infinitely thin bin or the limit of the pressure at a plane [22]. Practically, the extent of agreement in this exercise is limited by the inherent assumptions and spatial resolution of the two methods; a single average over a volume is required for VA, but a linear pressure relationship is assumed for CV to obtain the pressure tensor value corresponding to the center of the CV.

The continuum analytical xy pressure tensor component can be derived analytically using the same Fourier series approach for $\partial u_x/\partial y$ [55],

$$\Pi_{xy}(y,t) = -\frac{\mu U_0}{L}\left[1 + 2\sum_{n=1}^{\infty}(-1)^n e^{-\frac{\lambda_n \mu t}{\rho}}\cos\left(\frac{n\pi y}{L}\right)\right], \tag{73}$$

which is valid for the entire domain $0 \leqslant y \leqslant L$.

A statistically meaningful comparison among the CV, VA, and continuum analytic shear pressure profiles requires more averaging of the simulation data than for the streaming velocity [57] and eight independent simulation trajectories over five reduced time units were used. Figure 11 shows that the three methods exhibit good agreement within the simulation statistical uncertainty.

As a final demonstration of the use of the CV equations, the control volume is now chosen to encompass the entire liquid domain (see Fig. 8), and, therefore, the external forces arise from interactions with the wall atoms only. The momentum

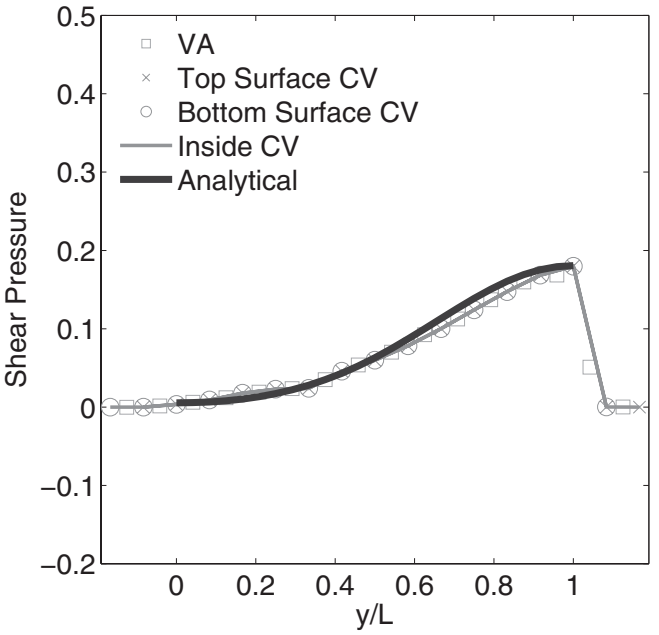

FIG. 11. As Fig. 10, except that the NEMD results are averaged over a set of eight independent simulations of 1000 time steps (five reduced time units) each. The simulation-derived VA and CV shear pressures are compared with the continuum analytical solution given in Eq. (73) (solid black line). The jump in the profile on the right of the figure is due to the presence of the tethered wall.

equation, Eq. (55), is written as

$$\frac{\partial}{\partial t}\sum_{i=1}^{N}\mathbf{p}_i\vartheta_i = -\sum_{i=1}^{N}\overbrace{\frac{\mathbf{p}_i\mathbf{p}_i}{m_i}\cdot d\mathbf{S}_i}^{①} + \sum_{i=1}^{N}\overbrace{\mathbf{f}_{i_{\text{ext}}}\vartheta_i}^{③} - \frac{1}{2}\sum_{i,j}^{N}\Big[\underbrace{\mathbf{f}_{ij}dS_{xij}}_{②} + \underbrace{\mathbf{f}_{ij}}_{④}dS_{yij} + \underbrace{\mathbf{f}_{ij}dS_{zij}}_{②}\Big],$$

which can be simplified as follows. For term ① in the above equation, the fluxes across the CV boundaries in the streamwise and spanwise directions cancel due to the periodic boundary conditions. Fluxes across the xz boundary surface are zero as the tethered wall atoms prevent such crossings. The force term ② also vanishes because across the periodic boundary, $\mathbf{f}_{ij}dS^{+}_{xij} = -\mathbf{f}_{ij}dS^{-}_{xij}$ (similarly for z). The external force term ③ is zero because all the forces in the system result from interatomic interactions. The sum of the f_{yij} force components across the horizontal boundaries will be equal and opposite, and, by symmetry, the two f_{zij} terms in ④ will be zero on average. The above equation therefore reduces to

$$\frac{\partial}{\partial t}\sum_{i=1}^{N}\mathbf{p}_i\vartheta_i = -\frac{1}{2}\sum_{i,j}^{N}[f_{xij}dS^{+}_{yij} - f_{xij}dS^{-}_{yij}]. \tag{74}$$

As the simulation approaches steady state, the rate of change of momentum in the control volume tends to zero because the difference between the shear stresses acting across the top and bottom walls vanishes. The forces on the xz plane boundary and momentum inside the CV are plotted in Fig. 12 to confirm Eq. (74) numerically. The time evolution of these molecular momenta and surface stresses are compared to the analytical

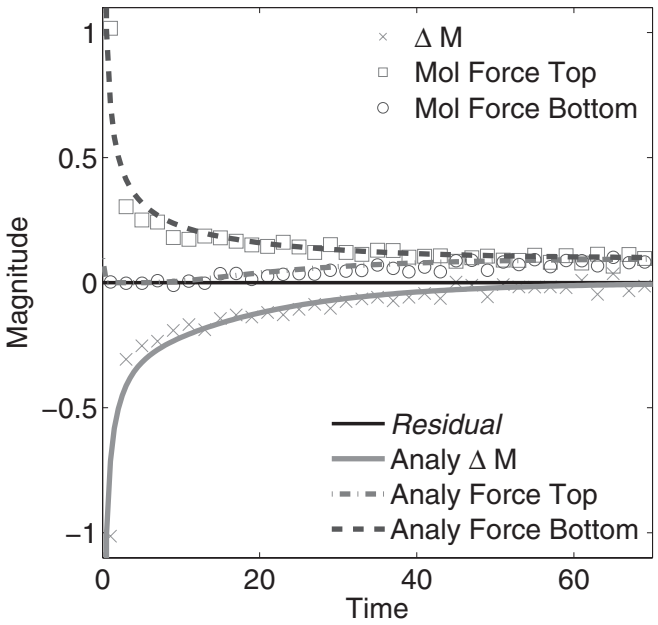

FIG. 12. The evolution of surface forces and momentum change for a molecular CV from Eq. (74), (points) and analytical solution for the continuum Eqs. (76)–(78), presented as lines on the figure. The Residual, defined in Eq. (66), is also given. Each point represents the average over an ensemble of eight independent systems and 40 time steps.

continuum solution for the CV,

$$\frac{\partial}{\partial t}\int_V \rho u_x dV = -\left[\int_{S_f^+} \Pi_{xy} dS_f^+ - \int_{S_f^-} \Pi_{xy} dS_f^-\right]. \quad (75)$$

The normal components of the pressure tensor are nonzero in the continuum, but exactly balance across opposite CV faces, i.e., $\Pi_{xx}^+ = \Pi_{xx}^-$. By appropriate choice of the gauge pressure, Π_{xx} does not appear in the governing Eq. (75). The left-hand side of the above equation is evaluated from the analytic expression for u_x,

$$\frac{\partial}{\partial t}\int_V \rho u_x dV = 2\Delta x \Delta z \frac{\mu U_0}{L} \sum_{n=1}^{\infty} [1-(-1)^n] e^{-\frac{\lambda_n \mu t}{\rho}}. \quad (76)$$

The right-hand side is obtained from the analytic continuum expression for the shear stress, for the bottom surface at $y = 0$,

$$\int_{S_f^+} \Pi_{xy} dS_f^+ = -2\Delta x \Delta z \frac{\mu U_0}{L} \sum_{n=1}^{\infty} e^{-\frac{\lambda_n \mu t}{\rho}}, \quad (77)$$

and for the top $y = L$,

$$\int_{S_f^-} \Pi_{xy} dS_f^- = -2\Delta x \Delta z \frac{\mu U_0}{L} \sum_{n=1}^{\infty} (-1)^n e^{-\frac{\lambda_n \mu t}{\rho}}. \quad (78)$$

In Fig. 12, the momentum evolution on the left-hand side of Eq. (74) is compared to Eq. (76). Equations (77) and (78) are also given for the shear stresses acting across the top and bottom of the molecular control volume [right-hand side of Eq. (74)]. The scatter seen in the MD data reflects the thermal fluctuations in the forces and molecular crossings of the CV boundaries. The average response nevertheless agrees well with the analytic solution, bearing in mind the element of uncertainty in the matching state parameter values. This example demonstrates the potential of the CV approach applied on the molecular scale, as it can be seen that computation of the forces across the CV boundaries determines completely the average molecular microhydrodynamic response of the system contained in the CV. In fact, the force on only one of the surfaces is all that was required, as the force terms for the opposite surface could have been obtained from Eq. (74).

V. CONCLUSIONS

In analogy to continuum fluid mechanics, the evolution equations for a molecular systems has been expressed within a CV in terms of fluxes and stresses across the surfaces. A key ingredient is the definition and manipulation of a Lagrangian to control volume conversion function, ϑ, which identifies molecules within the CV. The final appearance of the equations has the same form as Reynolds' transport theorem applied to a discrete system. The equations presented follow directly from Newton's equation of motion for a system of discrete particles, requiring no additional assumptions and, therefore, sharing the same range of validity. Using the $\mathcal{LCV}$ function, the relationship between VA [16,17] and MOP pressure [13,14] has been established without Fourier transformation. The two definitions of pressure are shown numerically to give equivalent results away from equilibrium and, for homogeneous systems, shown to equal the virial pressure.

A Navier–Stokes-like equation was derived for the evolution of momentum within the control volume, expressed in terms of surface fluxes and stresses. This provides an exact mathematical relationship between molecular fluxes and pressures and the evolution of momentum and energy in a CV. Numerical evaluations of the terms in the conservation of mass, momentum, and energy equations demonstrated consistency with theoretical predictions.

The CV formulation is general and can be applied to derive conservation equations for any fluid dynamical property localized to a region in space. It can also facilitate the derivation of conservative numerical schemes for MD, and the evaluation of the accuracy of numerical schemes. Finally, it allows for accurate evaluation of macroscopic flow properties in a manner consistent with the continuum conservation laws.

APPENDIX A: DISCRETE FORM OF REYNOLDS' TRANSPORT THEOREM AND THE DIVERGENCE THEOREM

In this Appendix, both Reynolds' transport theorem and the divergence theorem for a discrete system are derived. The relationship between an advecting and fixed control volume is shown using the concept of peculiar momentum.

The microscopic form of the continuous Reynolds' transport theorem [1] is derived for a property $\boldsymbol{\chi} = \boldsymbol{\chi}(\mathbf{r}_i, \mathbf{p}_i, t)$ which could be mass, momentum, or the pressure tensor. The $\mathcal{LCV}$ function, ϑ_i, is dependent on the molecule's coordinate; the location of the cube center, $\mathbf{r}$, and side length, $\Delta\mathbf{r}$, which are all a function of time. The time evolution of the CV is,

therefore,

$$\frac{d}{dt}\sum_{i=1}^{N}\boldsymbol{\chi}(t)\vartheta_i[\mathbf{r}_i(t),\mathbf{r}(t),\Delta\mathbf{r}(t)] = \sum_{i=1}^{N}\left[\frac{d\boldsymbol{\chi}}{dt}\vartheta_i+\boldsymbol{\chi}\frac{d\mathbf{r}_i}{dt}\cdot\frac{\partial\vartheta_i}{\partial\mathbf{r}_i}+\boldsymbol{\chi}\frac{d\mathbf{r}}{dt}\cdot\frac{\partial\vartheta_i}{\partial\mathbf{r}}+\boldsymbol{\chi}\frac{d\Delta\mathbf{r}}{dt}\cdot\frac{\partial\vartheta_i}{\partial\Delta\mathbf{r}}\right].$$

The velocity of the moving volume is defined as $\tilde{\boldsymbol{u}} = d\mathbf{r}/dt$, which can differ from the macroscopic velocity $\boldsymbol{u}$. Surface translation or deformation of the cube, $\partial\vartheta_i/\partial\Delta\mathbf{r}$, can be included in the expression for velocity $\tilde{\boldsymbol{u}}$. The above analysis is for a microscopic system, although a similar process for a mesoscopic system can be applied and includes terms for CV movement in Eq. (12).

Hence, Reynolds treatment of a continuous medium [1] is extended here to a discrete molecular system,

$$\frac{d}{dt}\sum_{i=1}^{N}\boldsymbol{\chi}(t)\vartheta_i[\mathbf{r}_i(t),\mathbf{r}(t),\Delta\mathbf{r}(t)] = \sum_{i=1}^{N}\left[\frac{d\boldsymbol{\chi}}{dt}\vartheta_i+\boldsymbol{\chi}\left(\tilde{\boldsymbol{u}}-\frac{\mathbf{p}_i}{m_i}\right)\cdot d\mathbf{S}_i\right]. \tag{A1}$$

The conservation equation for the mass, $\boldsymbol{\chi} = m_i$, in a moving reference frame is

$$\frac{d}{dt}\sum_{i=1}^{N}m_i\vartheta_i = \sum_{i=1}^{N}\left[m_i\left(\tilde{\boldsymbol{u}}-\frac{\mathbf{p}_i}{m_i}\right)\cdot d\mathbf{S}_i\right]. \tag{A2}$$

In a Lagrangian reference frame, the translational velocity of CV surface must be equal to the molecular streaming velocity, i.e., $\tilde{\boldsymbol{u}}(\mathbf{r}^{\pm}) = \boldsymbol{u}(\mathbf{r}_i)$, so

$$\sum_{i=1}^{N}\left[m_i\left(\boldsymbol{u}-\frac{\mathbf{p}_i}{m_i}\right)\cdot d\mathbf{S}_i\right] = -\sum_{i=1}^{N}\overline{\mathbf{p}}_i\cdot d\mathbf{S}_i.$$

The evolution of the peculiar momentum, $\boldsymbol{\chi} = \overline{\mathbf{p}}_i$, in a moving reference frame is

$$\frac{d}{dt}\sum_{i=1}^{N}\overline{\mathbf{p}}_i\vartheta_i = \sum_{i=1}^{N}\left[\mathbf{F}_i\vartheta_i+\overline{\mathbf{p}}_i\left(\boldsymbol{u}-\frac{\mathbf{p}_i}{m_i}\right)\cdot d\mathbf{S}_i\right] = \sum_{i=1}^{N}\left[\mathbf{F}_i\vartheta_i-\frac{\overline{\mathbf{p}}_i\overline{\mathbf{p}}_i}{m_i}\cdot d\mathbf{S}_i\right].$$

Here an inertial reference frame has been assumed so $d\overline{\mathbf{p}}_i/dt = d\mathbf{p}_i/dt = \mathbf{F}_i$. For a simple case (e.g., one-dimensional flow) it is possible to utilize a Lagrangian description by ensuring $\tilde{\boldsymbol{u}}(\mathbf{r}^{\pm}) = \boldsymbol{u}(\mathbf{r}_i)$ throughout the time evolution. In more complicated cases, this is not always possible and the Eulerian description is generally adopted.

Next, a microscopic analog to the macroscopic divergence theorem is derived for the generalized function, $\boldsymbol{\chi}$,

$$\int_V\sum_{i=1}^{N}\frac{\partial}{\partial\mathbf{r}}\cdot[\boldsymbol{\chi}(\mathbf{r}_i,\mathbf{p}_i,t)\delta(\mathbf{r}_i-\mathbf{r})]dV = \int_V\sum_{i=1}^{N}\boldsymbol{\chi}(\mathbf{r}_i,\mathbf{p}_i,t)\cdot\frac{\partial}{\partial\mathbf{r}}\delta(\mathbf{r}_i-\mathbf{r})dV.$$

The vector derivative of the Dirac δ followed by the integral over volume results in

$$\int_V\frac{\partial}{\partial\mathbf{r}}\delta(x_i-x)\delta(y_i-y)\delta(z_i-z)dV = \begin{pmatrix}[\delta(x_i-x)H(y_i-y)H(z_i-z)]_V\\ [H(x_i-x)\delta(y_i-y)H(z_i-z)]_V\\ [H(x_i-x)H(y_i-y)\delta(z_i-z)]_V\end{pmatrix} = \begin{pmatrix}[\delta(x_i-x^+)-\delta(x_i-x^-)]S_{xi}\\ [\delta(y_i-y^+)-\delta(y_i-y^-)]S_{yi}\\ [\delta(z_i-z^+)-\delta(z_i-z^-)]S_{zi}\end{pmatrix} = d\mathbf{S}_i,$$

where the limits of the cuboidal volume are $\mathbf{r}^+ = \mathbf{r}+\frac{\Delta\mathbf{r}}{2}$ and $\mathbf{r}^- = \mathbf{r}-\frac{\Delta\mathbf{r}}{2}$. The mesoscopic equivalent of the continuum divergence theorem Eq. (5) is, therefore,

$$\int_V\frac{\partial}{\partial\mathbf{r}}\cdot\sum_{i=1}^{N}\boldsymbol{\chi}\delta(\mathbf{r}_i-\mathbf{r})dV = \sum_{i=1}^{N}\boldsymbol{\chi}\cdot d\mathbf{S}_i.$$

APPENDIX B: RELATION BETWEEN CONTROL VOLUME AND DESCRIPTION AT A POINT

This appendix proves that the Irving and Kirkwood [8] expression for the flux at a point is the zero volume limit of the CV formulation. As in the continuum, the control volume equations at a point are obtained using the gradient operator in Eq. (6). The flux at a point can be shown by taking the zero volume limit of the gradient operator of Eq. (6). Assuming the three side lengths of the control volume, Δx, Δy, and Δz, tend to zero and, hence, the volume, ΔV, tends to zero,

$$\boldsymbol{\nabla}\cdot\rho\boldsymbol{u} = \lim_{\Delta x\to0}\lim_{\Delta y\to0}\lim_{\Delta z\to0}\frac{1}{\Delta x\Delta y\Delta z}\times\sum_{i=1}^{N}\left\langle p_{ix}\frac{\partial\vartheta_i}{\partial x}+p_{iy}\frac{\partial\vartheta_i}{\partial y}+p_{iz}\frac{\partial\vartheta_i}{\partial z};f\right\rangle, \tag{B1}$$

from Eq. (21). For illustration, consider the x component above, where

$$\frac{\partial\vartheta_i}{\partial x} = \overbrace{[\delta(x^+-x_i)-\delta(x^--x_i)]}^{x_{\text{face}}}S_{xi}. \tag{B2}$$

Using the definition of the Dirac δ function as the limit of two slightly displaced Heaviside functions,

$$\delta(\xi) = \lim_{\Delta\xi\to0}\frac{H\left(\xi+\frac{\Delta\xi}{2}\right)-H\left(\xi-\frac{\Delta\xi}{2}\right)}{\Delta\xi},$$

the limit of the S_{xi} term is

$$\lim_{\Delta y\to0}\lim_{\Delta z\to0}S_{xi} = \delta(y_i-y)\delta(z_i-z).$$

The $\Delta x\to0$ limit for x_{face} [defined in Eq. (B2)] can be evaluated using L'Hôpital's rule, combined with the property of the δ function,

$$\frac{\partial}{\partial(\Delta\xi)}\delta\left(\xi-\frac{\Delta\xi}{2}\right) = -\frac{1}{2}\frac{\partial}{\partial\xi}\delta\left(\xi-\frac{\Delta\xi}{2}\right),$$

so

$$\lim_{\Delta x\to0}x_{\text{face}} = \frac{\partial}{\partial x}\delta(x-x_i).$$

Therefore, the limit of $\partial\vartheta_i/\partial x$ as the volume approaches zero is

$$\lim_{\Delta x\to 0}\lim_{\Delta y\to 0}\lim_{\Delta z\to 0}\frac{\partial\vartheta_i}{\partial x}=\frac{\partial}{\partial x}\delta(\mathbf{r}_i-\mathbf{r}).$$

Taking the limits for the x, y, and z terms in Eq. (B1) yields the expected Irving and Kirkwood [8] definition of the divergence at a point,

$$\nabla\cdot\rho\boldsymbol{u}=\sum_{i=1}^{N}\left\langle\frac{\partial}{\partial\mathbf{r}}\cdot\mathbf{p}_i\delta(\boldsymbol{r}_i-\boldsymbol{r});f\right\rangle.$$

This zero volume limit of the CV surface fluxes shows that the divergence of a Dirac δ function represents the flow of molecules over a point in space. The advection and kinetic pressure at a point is, from Eq. (25),

$$\nabla\cdot[\rho\boldsymbol{u}\boldsymbol{u}+\boldsymbol{\kappa}]=\sum_{i=1}^{N}\left\langle\frac{\partial}{\partial\mathbf{r}}\cdot\frac{\mathbf{p}_i\mathbf{p}_i}{m_i}\delta(\boldsymbol{r}_i-\boldsymbol{r});f\right\rangle.$$

The same limit of zero volume for the surface tractions defines the Cauchy stress. Using Eq. (6) and taking the limit of Eq. (46), written in terms of tractions,

$$\begin{aligned}\nabla\cdot\boldsymbol{\sigma}&=\lim_{\Delta V\to 0}\frac{1}{\Delta V}\sum_{\text{faces}}^{6}\int_{S_f}\boldsymbol{\sigma}\cdot d\mathbf{S}_f\\&=\lim_{\Delta r_x\to 0}\lim_{\Delta r_y\to 0}\lim_{\Delta r_z\to 0}\left[\frac{\mathbf{T}_x^+-\mathbf{T}_x^-}{\Delta r_x}\right.\\&\quad\left.+\frac{\mathbf{T}_y^+-\mathbf{T}_y^-}{\Delta r_y}+\frac{\mathbf{T}_z^+-\mathbf{T}_z^-}{\Delta r_z}\right].\end{aligned}$$

For the r_x^+ surface, and taking the limits of Δr_y and Δr_z using L'Hôpital's rule,

$$\lim_{\Delta V\to 0}\frac{\mathbf{T}_x^+}{\Delta r_x}=-\lim_{\Delta r_x\to 0}\frac{1}{2\Delta r_x}\sum_{i,j}^{N}\langle f_{\alpha ij}\varpi_{xyz}^{+};f\rangle,$$

where ϖ is

$$\begin{aligned}\varpi_{\beta\kappa\gamma}^{\dagger}\equiv&[H(r_\beta^\dagger-r_{\beta j})-H(r_\beta^\dagger-r_{\beta i})]\\&\times\delta\left[r_\kappa-r_{\kappa i}-\frac{r_{\kappa ij}}{r_{\beta ij}}(r_\beta^\dagger-r_{\beta i})\right]\\&\times\delta\left[r_\gamma-r_{\gamma i}-\frac{r_{\gamma ij}}{r_{\beta ij}}(r_\beta^\dagger-r_{\beta i})\right].\end{aligned}\tag{B3}$$

The indices β, κ, and γ can be x, y, or z and $\dagger$ denotes the top surface ($+$ superscript), bottom surface ($-$ superscript), or CV center (no superscript). The ϖ selecting function includes only the contribution to the stress when the line of interaction between i and j passes through the point $\mathbf{r}^\dagger$ in space. The difference between $\mathbf{T}_x^+$ and $\mathbf{T}_x^-$ tends to zero on taking the limit $\Delta r_x\to 0$, so L'Hôpital's rule can be applied. Using the property

$$\begin{aligned}&\frac{\partial}{\partial(\Delta\xi)}\delta\left(\xi-\frac{1}{2}\Delta\xi\right)H\left(\xi-\frac{1}{2}\Delta\xi\right)\\&\quad=-\frac{1}{2}\frac{\partial}{\partial\xi}\delta\left(\xi-\frac{1}{2}\Delta\xi\right)H\left(\xi-\frac{1}{2}\Delta\xi\right),\end{aligned}$$

then

$$\lim_{\Delta V\to 0}\frac{\mathbf{T}_x^+-\mathbf{T}_x^-}{\Delta r_x}=-\frac{1}{2}\sum_{i,j}^{N}\left\langle f_{\alpha ij}\frac{\partial\varpi_{xyz}}{\partial r_x};f\right\rangle,$$

where $r^+\to r$ and $r^-\to r$. The $\varpi_{\beta\kappa\gamma}$ function is the integral between two molecules introduced in Eq. (37),

$$\begin{aligned}&\int_0^1\delta(\mathbf{r}-\mathbf{r}_i+s\mathbf{r}_{ij})ds\\&\quad=\operatorname{sgn}\left(\frac{1}{r_{xij}}\right)\frac{1}{|r_{xij}|}[H(r_x-r_{xj})-H(r_x-r_{xi})]\\&\qquad\times\delta\left[r_y-r_{yi}-\frac{r_{yij}}{r_{xij}}(r_x-r_{xi})\right]\\&\qquad\times\delta\left[r_z-r_{zi}-\frac{r_{zij}}{r_{xij}}(r_x-r_{xi})\right].\end{aligned}$$

where the sifting property of the Dirac δ function in the r_x direction has been used to express the integral between two molecules in terms of the ϖ_{xyz} function. Hence,

$$\int_0^1\delta(\mathbf{r}-\mathbf{r}_i+s\mathbf{r}_{ij})ds=\frac{\varpi_{xyz}}{r_{xij}}.$$

As the choice of shifting direction is arbitrary, use of r_y or r_z in the above treatment would result in ϖ_{yzx} and ϖ_{zxy}, respectively. Therefore, Eq. (38), without the volume integral, can be expressed as

$$\begin{aligned}&\frac{1}{2}\sum_{i,j}^{N}\left\langle f_{\alpha ij}r_{\beta ij}\frac{\partial}{\partial r_\beta}\int_0^1\delta(\mathbf{r}-\mathbf{r}_i+s\mathbf{r}_{ij})ds;f\right\rangle\\&\quad=\frac{1}{2}\sum_{i,j}^{N}\left\langle f_{ij\alpha}\left[\frac{\partial\varpi_{xyz}}{\partial r_x}+\frac{\partial\varpi_{yxz}}{\partial r_y}+\frac{\partial\varpi_{zxy}}{\partial r_z}\right];f\right\rangle.\end{aligned}$$

As Eq. (38) is equivalent to the Irving and Kirkwood [8] stress of Eq. (36), the Irving Kirkwood stress is recovered in the limit that the CV tends to zero volume.

This Appendix has proved, therefore, that in the limit of zero control volume, the molecular CV Eqs. (22) and (49) recover the description at a point in the same limit that the continuum CV Eqs. (1) and (2) tend to the differential continuum equations. This demonstrates that the molecular CV equations presented here are the molecular scale equivalent of the continuum CV equations.

APPENDIX C: RELATIONSHIP BETWEEN VOLUME AVERAGE AND MOP STRESS

This appendix gives further details of the derivation of the MOP form of stress from the volume average form. Starting from Eq. (38) and written in terms of the CV function for an integrated volume,

$$\begin{aligned}-\sum_{\text{faces}}^{6}\int_{S_f}\boldsymbol{\sigma}\cdot d\mathbf{S}_f&=\frac{1}{2}\sum_{i,j}^{N}\left\langle\mathbf{f}_{ij}\mathbf{r}_{ij}\cdot\int_0^1\frac{\partial\vartheta_s}{\partial\mathbf{r}}ds;f\right\rangle\\&=\frac{1}{2}\sum_{i,j}^{N}\left\langle\mathbf{f}_{ij}\int_0^1\left[x_{ij}\frac{\partial\vartheta_s}{\partial x}+y_{ij}\frac{\partial\vartheta_s}{\partial y}+z_{ij}\frac{\partial\vartheta_s}{\partial z}\right]ds;f\right\rangle.\end{aligned}\tag{C1}$$

Taking only the x derivative above,

$$x_{ij}\frac{\partial \vartheta_s}{\partial x} = x_{ij}[\overbrace{\delta(x^+ - x_i + sx_{ij})}^{x^+_{\text{face}}} - \delta(x^- - x_i + sx_{ij})]G(s), \tag{C2}$$

where $G(s)$ is

$$G(s) \equiv [H(y^+ - y_i + sy_{ij}) - H(y^- - y_i + sy_{ij})] \times [H(z^+ - z_i + sz_{ij}) - H(z^- - z_i + sz_{ij})].$$

As $\delta(ax) = \frac{1}{|a|}\delta(x)$ the $x_{ij}x^+_{\text{face}}G(s)$ term in Eq. (C2) can be expressed as

$$x_{ij}x^+_{\text{face}}G(s) = \frac{x_{ij}}{|x_{ij}|}\delta\left(\frac{x^+ - x_i}{x_{ij}} + s\right)G(s). \tag{C3}$$

The integral can be evaluated using the sifting property of the Dirac δ function [58] as follows:

$$\begin{aligned}\int_0^1 x_{ij}x^+_{\text{face}}G(s)ds &= \frac{x_{ij}}{|x_{ij}|}\int_0^1 \delta\left(\frac{x^+ - x_i}{x_{ij}} + s\right)G(s)ds \\ &= \text{sgn}(x_{ij})\left[H\left(\frac{x^+ - x_j}{x_{ij}}\right) - H\left(\frac{x^+ - x_i}{x_{ij}}\right)\right]S^+_{xij}.\end{aligned}$$

where the signum function, $\text{sgn}(x_{ij}) \equiv x_{ij}/|x_{ij}|$. The S^+_{xij} term is the value of s on the cube surface, $S^+_{xij} = G(s = -\frac{x^+ - x_i}{x_{ij}})$, which is

$$\begin{aligned}S^+_{xij} \equiv &\left\{H\left[y^+ - y_i - \frac{y_{ij}}{x_{ij}}(x^+ - x_i)\right]\right. \\ &\left. - H\left[y^- - y_i - \frac{y_{ij}}{x_{ij}}(x^+ - x_i)\right]\right\} \\ &\times \left\{H\left[z^+ - z_i - \frac{z_{ij}}{x_{ij}}(x^+ - x_i)\right]\right. \\ &\left. - H\left[z^- - z_i - \frac{z_{ij}}{x_{ij}}(x^+ - x_i)\right]\right\}.\end{aligned} \tag{C4}$$

The definition S^+_{xij} [analogously to S_{xi} in Eq. (15)] has been introduced as it filters out those ij terms where the point of intersection of line r_{ij} and plane x^+ has y and z components between the limits of the cube surfaces. The corresponding terms, $S^\pm_{ij\alpha}$, are defined for $\alpha = \{y,z\}$. Taking $H(0) = \frac{1}{2}$, the Heaviside function can be rewritten as $H(ax) = \frac{1}{2}[\text{sgn}(a)\text{sgn}(x) - 1]$ and

$$\begin{aligned}&H\left(\frac{x^+ - x_j}{x_{ij}}\right) - H\left(\frac{x^+ - x_i}{x_{ij}}\right) \\ &\quad = \frac{1}{2}\text{sgn}\left(\frac{1}{x_{ij}}\right)[\text{sgn}(x^+ - x_j) - \text{sgn}(x^+ - x_i)],\end{aligned}$$

so the expression, $x_{ij}x^+_{\text{face}}G(s)$ in Eq. (C2) becomes

$$\begin{aligned}x_{ij}\int_0^1 x^+_{\text{face}}G(s)ds &= \frac{1}{2}\text{sgn}(x_{ij})\text{sgn}\left(\frac{1}{x_{ij}}\right)[\text{sgn}(x^+ - x_j) - \text{sgn}(x^+ - x_i)]S^+_{xij}.\end{aligned}$$

The signum function, $\text{sgn}(\frac{1}{x_{ij}})$, cancels the one obtained from integration along s, $\text{sgn}(x_{ij})$. The expression for the x^+ face is, therefore,

$$\begin{aligned}&-\int_{S^+_x} \boldsymbol{\sigma}\cdot d\mathbf{S}_{S^+_x} \\ &\quad = \frac{1}{2}\sum_{i,j}^N \left\langle \mathbf{f}_{ij}x_{ij}\int_0^1 x^+_{\text{face}}G(s)ds; f\right\rangle \\ &\quad = \frac{1}{4}\sum_{i,j}^N \langle \mathbf{f}_{ij}[\text{sgn}(x^+ - x_j) - \text{sgn}(x^+ - x_i)]S^+_{xij}; f\rangle.\end{aligned}$$

Repeating the same process for the other faces allows Eq. (C1) to be expressed as

$$\begin{aligned}\sum_{\text{faces}}^6 \int_{S_f} \boldsymbol{\sigma}\cdot d\mathbf{S}_f &= -\frac{1}{2}\sum_{i,j}^N \left\langle \mathbf{f}_{ij}\mathbf{r}_{ij}\cdot\int_0^1 \frac{\partial \vartheta_s}{\partial \mathbf{r}}ds; f\right\rangle \\ &= -\frac{1}{4}\sum_{i,j}^N \left\langle \mathbf{f}_{ij}\sum_{\alpha=1}^3 \tilde{n}_\alpha[dS^+_{\alpha ij} - dS^-_{\alpha ij}]; f\right\rangle,\end{aligned}$$

where $dS^\pm_{\alpha ij} \equiv \frac{1}{2}[\text{sgn}(r^\pm_\alpha - r_{\alpha j}) - \text{sgn}(r^\pm_\alpha - r_{\alpha i})]S^\pm_{\alpha ij}$ and $\tilde{n}_\alpha \equiv \text{sgn}(r_{\alpha ij})\text{sgn}(\frac{1}{r_{\alpha ij}}) = [1,1,1]$. This is the force over the CV surfaces, Eq. (46), in Sec. III C.

To verify the interpretation of S^+_{xij} used in this work, consider the vector equation for the point of intersection of a line and a plane in space. The equation for a vector $\mathbf{a}$ between $\mathbf{r}_i$ and $\mathbf{r}_j$ is defined as $\mathbf{a} = \mathbf{r}_i - s\frac{\mathbf{r}_{ij}}{|\mathbf{r}_{ij}|}$. The plane containing the positive face of a cube is defined by $(\mathbf{r}^+ - \mathbf{p})\cdot\mathbf{n}$, where $\mathbf{p}$ is any point on the plane and $\mathbf{n}$ is normal to that plane. By setting $\mathbf{a} = \mathbf{p}$ and on rearrangement of $(\mathbf{r}^+ - \mathbf{r}_i + s\frac{\mathbf{r}_{ij}}{|\mathbf{r}_{ij}|})\cdot\mathbf{n}$, the value of s at the point of intersection with the plane is

$$s = -\frac{(\mathbf{r}^+ - \mathbf{r}_i)\cdot\mathbf{n}}{\frac{\mathbf{r}_{ij}}{|\mathbf{r}_{ij}|}\cdot\mathbf{n}}.$$

The point on line $\mathbf{a}$ located on the plane is

$$\mathbf{a}^+_p \equiv \mathbf{r}_i + \mathbf{r}_{ij}\left[\frac{(\mathbf{r}^+ - \mathbf{r}_i)\cdot\mathbf{n}}{\mathbf{r}_{ij}\cdot\mathbf{n}}\right].$$

Taking $\mathbf{n}$ as the normal to the x surface, i.e., $\mathbf{n} \to \mathbf{n}_x = [1,0,0]$, then,

$$x^+_{\alpha p} = \begin{pmatrix} x^+_{xp} \\ x^+_{yp} \\ x^+_{zp}\end{pmatrix} = \begin{bmatrix} x^+ \\ y_i + \frac{y_{ij}}{x_{ij}}(x^+ - x_i) \\ z_i + \frac{z_{ij}}{x_{ij}}(x^+ - x_i)\end{bmatrix},$$

written using index notation with $\alpha = \{x,y,z\}$. The vector $\mathbf{x}^+_p$ is the point of intersection of line $\mathbf{a}$ with the x^+ plane. A function to check if the point $\mathbf{x}^+_p$ on the plane is located on the region between $y^\pm$ and $z^\pm$, would use Heaviside functions and is similar to the form of Eq. (15),

$$\begin{aligned}S^+_{xij} = &[H(y^+ - \mathbf{x}^+_{yp}) - H(y^- - \mathbf{x}^+_{yp})] \\ &\times [H(z^+ - \mathbf{x}^+_{zp}) - H(z^- - \mathbf{x}^+_{zp})],\end{aligned}$$

which is the form obtained in the text by direct integration of the expression for stress, i.e., Eq. (C4).

[1] O. Reynolds, *Papers on Mechanical and Physical Subjects*, 1st ed., Vol. 3 (Cambridge University Press, Cambridge, 1903).
[2] T. A. Zaki and P. A. Durbin, J. Fluid Mech. **531**, 85 (2005).
[3] T. A. Zaki and P. A. Durbin, J. Fluid Mech. **563**, 357 (2006).
[4] C. Hirsch, *Numerical Computation of Internal and External Flows*, 2nd ed. (Elsevier, Oxford, 2007).
[5] M. Rosenfeld, D. Kwak, and M. Vinokur, J. Comput. Phys. **94**, 102 (1991).
[6] T. A. Zaki, J. G. Wissink, W. Rodi, and P. A. Durbin, J. Fluid Mech. **665**, 57 (2010).
[7] D. J. Evans and G. P. Morriss, *Statistical Mechanics of Non-Equilibrium Liquids*, 2nd ed. (Australian National University Press, Canberra, 2007).
[8] J. H. Irving and J. G. Kirkwood, J. Chem. Phys. **18**, 817 (1950).
[9] M. Zhou, Proc. R. Soc. London **459**, 2347 (2003).
[10] E. N. Parker, Phys. Rev. **96**, 1686 (1954).
[11] W. Noll, Phys. Rev. **96**, 1686 (1954).
[12] D. H. Tsai, J. Chem. Phys. **70**, 1375 (1978).
[13] B. D. Todd, D. J. Evans, and P. J. Daivis, Phys. Rev. E **52**, 1627 (1995).
[14] M. Han and J. S. Lee, Phys. Rev. E **70**, 061205 (2004).
[15] R. J. Hardy, J. Chem. Phys. **76**, 622 (1982).
[16] J. F. Lutsko, J. Appl. Phys. **64**, 1152 (1988).
[17] J. Cormier, J. M. Rickman, and T. J. Delph, J. Appl. Phys. **89**, 99 (2001).
[18] A. I. Murdoch, J. Elast. **88**, 113 (2007).
[19] A. I. Murdoch, J. Elast. **100**, 33 (2010).
[20] P. Schofield and J. R. Henderson, Proc. R. Soc. London A **379**, 231 (1982).
[21] N. C. Admal and E. B. Tadmor, J. Elast. **100**, 63 (2010).
[22] D. M. Heyes, E. R. Smith, D. Dini, and T. A. Zaki, J. Chem. Phys. **135**, 024512 (2011).
[23] S. T. O'Connell and P. A. Thompson, Phys. Rev. E **52**, R5792 (1995).
[24] N. G. Hadjiconstantinou, Ph.D. thesis, MIT, 1998.
[25] J. Li, D. Liao, and S. Yip, Phys. Rev. E **57**, 7259 (1998).
[26] N. G. Hadjiconstantinou, J. Comput. Phys. **154**, 245 (1999).
[27] E. G. Flekkøy, G. Wagner, and J. Feder, Europhys. Lett. **52**, 271 (2000).
[28] G. Wagner, E. Flekkøy, J. Feder, and T. Jossang, Comput. Phys. Commun. **147**, 670 (2002).
[29] R. Delgado-Buscalioni and P. V. Coveney, Phys. Rev. E **67**, 046704 (2003).
[30] W. A. Curtin and R. E. Miller, Modell. Simul. Mater. Sci. Eng. **11**, R33 (2003).
[31] X. B. Nie, S. Y. Chen, W. N. E, and M. O. Robbins, J. Fluid Mech. **500**, 55 (2004).
[32] T. Werder, J. H. Walther, and P. Koumoutsakos, J. Comput. Phys. **205**, 373 (2005).
[33] W. Ren, J. Comput. Phys. **227**, 1353 (2007).
[34] M. K. Borg, G. B. Macpherson, and J. M. Reese, Molec. Sims. **36**, 745 (2010).
[35] A. I. Borisenko and I. E. Tarapov, *Vector and Tensor Analysis with Applications*, 2nd ed. (Dover, New York, 1979).
[36] W. Humphrey, A. Dalke, and K. Schulten, J. Mol. Graphics **14**, 33 (1996).
[37] The cuboid is chosen as the most commonly used shape in continuum mechanic simulations on structured grids, although the process could be applied to any arbitrary shape.
[38] M. Serrano and P. Español, Phys. Rev. E **64**, 046115 (2001).
[39] A. K. Subramaniyan and C. T. Sun, J. Elast. **88**, 113 (2007).
[40] W. G. Hoover, C. G. Hoover, and J. F. Lutsko, Phys. Rev. E **79**, 036709 (2009).
[41] The resulting equality satisfies Eq. (39) and both sides are equal to within an arbitrary constant (related to choosing the gauge).
[42] S. Nemat-Nasser, *Plasticity: A Treatise on the Finite Deformation of Heterogeneous Inelastic Materials*, 1st ed. (Cambridge University Press, Cambridge, 2004).
[43] K. M. Mohamed and A. A. Mohamad, Microfluid. Nanofluid. **8**, 283 (2009).
[44] R. Delgado-Buscalioni, Lect. Notes.Comp. Sci. **82**, 145 (2012).
[45] R. Delgado-Buscalioni and P. Coveney, Philos. Trans. R. Soc. London **362**, 1639 (2004).
[46] G. DeFabritiis, R. Delgado-Buscalioni, and P. V. Coveney, Phys. Rev. Lett. **97**, 134501 (2006).
[47] O. Zienkiewicz, *The Finite Element Method: Its Basis and Fundamentals*, 6th ed. (Elsevier Butterworth-Heinemann, Oxford, 2005).
[48] P. J. Daivis, K. P. Travis, and B. D. Todd, J. Chem. Phys. **104**, 9651 (1996).
[49] M. P. Allen and D. J. Tildesley, *Computer Simulation of Liquids*, 1st ed. (Clarendon Press, Oxford, 1987).
[50] D. C. Rapaport, *The Art of Molecular Dynamics Simulation*, 2nd ed. (Cambridge University Press, Cambridge, 2004).
[51] R. Delgado-Buscalioni and G. DeFabritiis, Phys. Rev. E **76**, 036709 (2007).
[52] W. G. Hoover, *Computational Statistical Mechanics*, 1st ed. (Elsevier Science, Oxford, 1991).
[53] J. Petravic and P. Harrowell, J. Chem. Phys. **124**, 014103 (2006).
[54] M. C. Potter and D. C. Wiggert, *Mechanics of Fluids*, 3rd ed. (Brooks/Cole, California, 2002).
[55] W. A. Strauss, *Partial Differential Equations*, 1st ed. (John Wiley & Sons, New Jersey, 1992).
[56] F. Da Costa Silva, L. A. F. Coelho, F. W. Tavares, and M. J. E. M. Cardoso, Int. J. Quantum Chem. **95**, 79 (2003).
[57] N. G. Hadjiconstantinou, A. L. Garcia, M. Z. Bazant, and G. He, J. Comput. Phys. **187**, 274 (2003).
[58] V. Thankoppan, *Quantum Mechanics*, 1st ed. (New Age, New Delhi, 1985).